https://doi.org/10.5194/cp-2021-136
Preprint. Discussion started: 14 October 2021

Climate of the Past Discussions

Orbital Insolation Variations, Intrinsic Climate Variability, and Quaternary Glaciations

Keno Riechers[1,2], Takahito Mitsui[1,2], Niklas Boers[2,3,4], and Michael Ghil[5,6]

[1]Department of Mathematics and Computer Science, Freie Universität Berlin, Berlin, Germany
[2]Potsdam Institute for Climate Impact Research, Potsdam, Germany
[3]Earth System Modelling, School of Engeneering & Design, Technical University of Munich, Munich, Germany
[4]Department of Mathematics and Global Systems Institute, University of Exeter, Exeter, UK
[5]Geosciences Department and Laboratoire de Météorologie Dynamique (CNRS and IPSL), Ecole Normale Supérieure and PSL University, Paris, France
[6]Department of Atmospheric and Oceanic Science, University of California at Los Angeles, Los Angeles, United States

Correspondence: Keno Riechers (riechers@pik-potsdam.de)

Abstract. The relative role of external forcing and of intrinsic variability is a key question of climate variability in general and of our planet's paleoclimatic past in particular. Over the last 100 years since Milankovitch's contributions, the role of orbital forcing has been well established for the last 2.6 Myr and their Quaternary glaciation cycles. A convincing case has also been made for the role of several internal mechanisms that are active on time scales both shorter and longer than the orbital ones. Such mechanisms clearly have a causal role in Dansgaard-Oeschger and Heinrich events, as well as in the mid-Pleistocene transition. We introduce herein a unified framework for the understanding of the interplay between internal mechanisms and orbital forcing on time scales from thousands to millions of years. This framework relies on the fairly recent theory of nonautonomous and random dynamical systems and it has been successfully applied so far in the climate sciences for problems like the El Niño-Southern Oscillation, the oceans' wind-driven circulation, and other problems on interannual to interdecadal time scales. Finally, we provide further examples of climate applications and present preliminary results of interest for the Quaternary glaciation cycles in general and the mid-Pleistocene transition in particular.

1 INTRODUCTION AND MOTIVATION

For two centuries or more of modern geology, records of our planet's physical and biological past were merely discrete sequences of strata with specific properties, like coloration and composition (Imbrie and Imbrie, 1986). This state of affairs led, after the initial success of the Milankovitch (1920) theory of the ice ages, to severe criticism of the mismatch between insolation minima and glaciation maxima (e.g., Flint, 1971).

The advent of marine-sediment cores after World War II led, for the first time, to the availability of records that were, more or less, continuous in time. Like all climate records, these cores covered limited time intervals and did so with limited resolution and with inaccuracies in absolute dating, as well as in the quantities being measured. Moreover, they posed the problem of inverting proxy records of isotopic and microbiotic counts to physical quantities like temperature and precipitation.

https://doi.org/10.5194/cp-2021-136
Preprint. Discussion started: 14 October 2021

Climate of the Past Discussions

In spite of these limitations, the spectral analysis of deep-sea records allowed Hays et al. (1976) to overcome the difficulties previously encountered by the orbital theory of Quaternary glaciations, in particular the absence of the imprint of precesional and obliquity peaks. Specifically, Hays et al. (1976) were able to create a composite record — back to over 400 kyr b2k, i.e., over 400 000 yr before the year 2000 A.D. — from two relatively long marine-sediment records of the best quality available in the early 1970s. The authors demonstrated therewith that precessional and obliquity peaks near 20 kyr and 40 kyr were present in this record's spectral analysis; see Fig. 1. The power spectrum in the figure also made it quite clear that these peaks were superimposed on a continuous background — the stippled area in the figure — whose total variance much exceeded the sum of the variances present in the peaks.

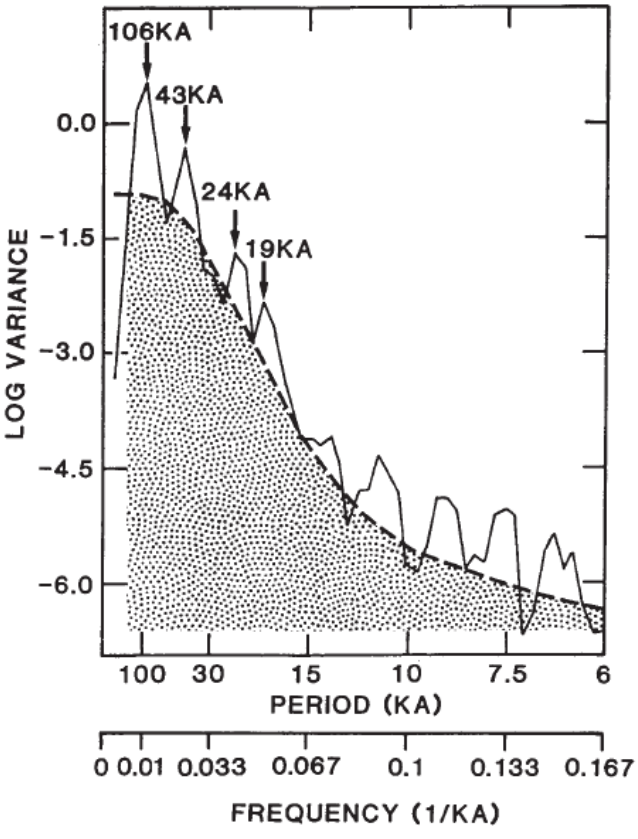

Figure 1. Power spectrum of a composite δ^{18}O record using deep-sea cores RC11-120 and E49-18. This figure is based on the work of Hays et al. (1976), as presented by Imbrie and Imbrie (1986). From Ghil and Childress (1987) with permission from Springer Science+Business Media.

The work of Hays et al. (1976) and of the subsequent CLIMAP and SPECMAP projects resulted in a much more detailed spatio-temporal mapping of the Quaternary and extended the belief in the pacemaking role of orbital variations into the more remote past. At the same time, the advent of higher-resolution marine cores and, especially, ice cores from both Greenland an

https://doi.org/10.5194/cp-2021-136
Preprint. Discussion started: 14 October 2021

Climate of the Past Discussions
Open Access
EGU

the Antarctica, led to the discovery of Heinrich events (Heinrich, 1988), Dansgaard-Oeschger (D-O) events (e.g., Dansgaard et al., 1993) and Bond cycles (Bond et al., 1997) that were hard to explain by orbital forcing, given their shorter time scales.

In fact, interest in past climates was heightened not only by these striking observational discoveries, but also by the growing concerns about humanity's impact on the climate (SMIC, 1971; National Research Council, 1975). Given the declining temperatures between the 1940s and 1970s — on the one hand, as shown in Fig. 2[1] — and the substantial advances in the description of the Quaternary glaciations, on the other, that interest was mainly in the planet's falling into another ice age (e.g., National Research Council, 1975).

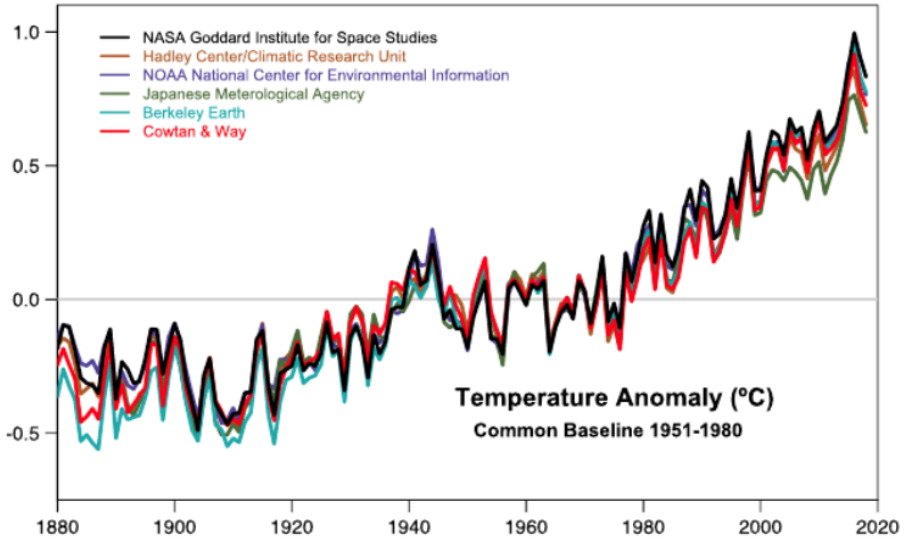

Figure 2. Comparison of six analyses of the annually and globally averaged surface temperature anomalies through 2018. NASA = National Aeronautics and Space Administration; NOAA = National Oceanic and Atmospheric Administration. Reproduced from Lenssen et al. (2019, Fig. 1) with permission from Wiley.

As a result of the twofold stimulation provided by data about past glaciations and concern about future ones, a number of researchers in the early-to-mid 1970s worked on energy balance models (EBMs) of climate with multiple stable steady states (Held and Suarez, 1974; North, 1975; Ghil, 1976). Two such stable "equilibria" corresponded to the present climate and to a "deep-freeze," as it was called at the time, i.e., to a totally ice-covered Earth. At the time there was some disbelief about this second climate, as its temperatures were much lower than those associated with the Quaternary glaciations and incompatible with paleoclimatic evidence available in the 1970s.

New geochemical evidence, though, led in the early 1990s to the discovery of a snowball or, at least, slushball Earth prior to the emergence of multicellular life, sometime before 650 Myr b2k (Hoffman et al., 1998). It thus turned out that this climate state — predicted by several EBMs, and confirmed by a general circulation model (GCM) with much higher spatial resolution

[1] see also Ghil and Vautard (1991, Fig. 3)

https://doi.org/10.5194/cp-2021-136
Preprint. Discussion started: 14 October 2021


Climate of the Past Discussions

(Wetherald and Manabe, 1975) — had actually occurred and it is now being modeled in much greater detail (Pierrehumbert, 2004; Ghil and Lucarini, 2020).

On the other hand, it also became clear that a model whose only stable solutions were stationary, could not reproduce very well the wealth of variability that the proxy records were describing. Certain theoretical paleoclimatologists turned, therefore, to coupling a "climate" equation, with temperature as its only dependent variable, with an ice-sheet equation (Källén et al., 1979; Ghil and Le Treut, 1981) or a carbon-dioxide equation (Saltzman et al., 1981; Saltzman and Maasch, 1988).

These coupled climate models, albeit highly idealized, did produce oscillatory solutions that captured some of the features of the Quaternary glaciation cycles as known at that time. For instance, the models of Ghil and associates (Källén et al., 1979; Ghil and Le Treut, 1981) captured the phase differences between peak ice sheet extent and minimum temperatures suggested by Ruddiman and McIntyre (1981) in the North Atlantic, while the work of Saltzman and associates (e.g., Saltzman and Maasch, 1988) captured the asymmetry of the glaciation cycles with their more rapid "terminations" (Broecker and Van Donk, 1970).

The stable self-sustained oscillations of these coupled models, though, were totally independent of any orbital or other time-dependent forcing, i.e. the solar input to their radiative budget was constant in time. Hence, they could not capture the wealth of spectral features, with their orbital and other peaks, of the paleorecords available by the 1980s. The basic quandary of the Quaternary glaciation cycles — at least from the point of view of theoretical climate dynamics (Ghil and Childress, 1987, Part IV) — is formulated in Fig. 3 below; see also Ghil (1994).

In this paper, we try to show a path toward resolving the four fundamental questions listed in the box below. In the next section, we summarize existing results on how the climate system's intrinsic variability arises at Quaternary time scales and on how this variability interacts with the time-dependent orbital forcing. In section 3, we outline a more general framework for the study of such interactions, as given by the theory of nonautonomous and random dynamical systems (NDSs and RDSs), and sketch an application of this theory to other climate problems. An application to the problem at hand is proposed in Sec. 4 and conclusions follow in Sec. 5.

2 SELF-SUSTAINED CLIMATE OSCILLATORS

2.1 A Simple Mechanism for Climate Oscillations

We follow Ghil (1994) in sketching the simplest physical mechanism for a self-sustained climate oscillation at fixed insolation forcing. Consider the Källén et al. (1979, KCG hereafter) oscillator, the first such self-sustained climate oscillator, to the best of our knowledge. The model itself was built from the ground up, coupling a scalar version of the Ghil (1976) energy balance model (EBM) with a simplified, scalar version of the Weertman (1964, 1976) ice sheet model (ISM). The model's details and further analyses of its ingredients and variants can be found in several references (e.g., Crafoord and Källén, 1978; Ghil and Tavantzis, 1983; Ghil, 1984; Bódai et al., 2015)

https://doi.org/10.5194/cp-2021-136
Preprint. Discussion started: 14 October 2021

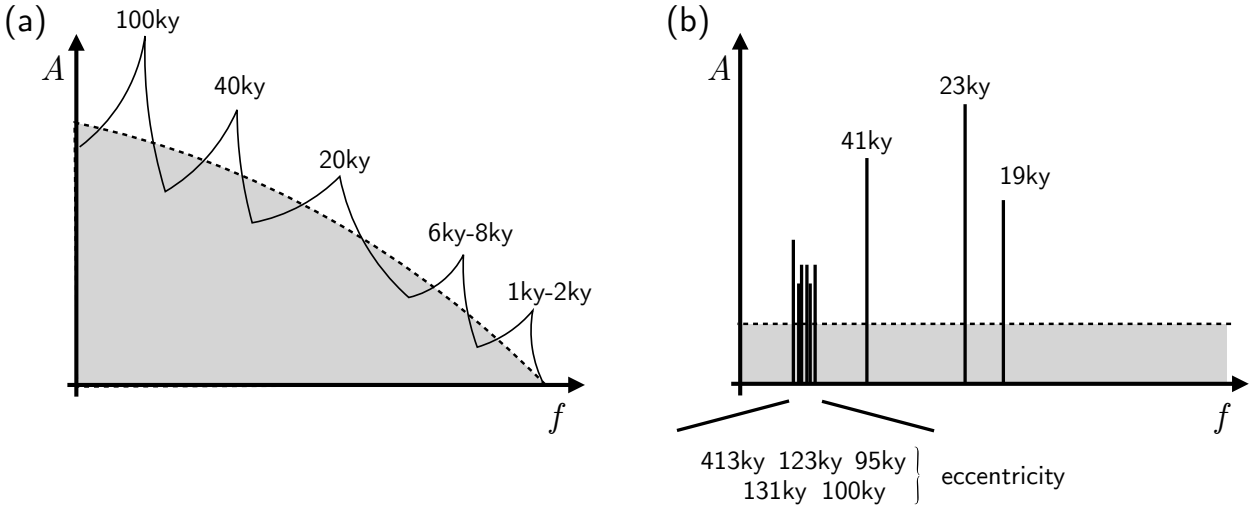

Figure 3. The theoretical quandary of modeling the Quaternary glaciation cycles, illustrated here by schematic diagrams of the composite power spectra of (a) the paleorecords and (b) the orbital forcing. In panel (a), the dominant peak for the Late Pleistocene is near 100 kyr, while in panel (b) eccentricity forcing is distributed over several spectral lines. The peaks at 6–8 kyr and 1–2 kyr in panel (a) correspond to Bond cycles (Bond et al., 1992, 1993) and to the mean recurrence of D-O events and they lack a match in the forcing lines of panel (b). Courtesy of N. Boers.

Based on the discussion so far and on the discrepancy between panels (a) and (b) of Fig. 3, we propose herein the following questions that need to be resolved, still, for a thorough understanding of Quaternary climate variability:

1. How does the dominant peak of the observed variability near 100 kyr arise, given the rather diffuse orbital forcing at this periodicity?
2. What causes the continuous part of the observed spectrum, which contains most of the variance?
3. What gives rise to the high-frequency peaks due to the sudden warmings and to the approximate periodicities associated with Heinrich and D-O events, among others?
4. What are the contributions of the orbital forcing and of the climate system's intrinsic variability to items (1)–(3) and how exactly do the two interact?

Box 1. Fundamental questions regarding the Quaternary glacial-interglacial cycles.

The basic workings of this climate oscillator can be represented by two coupled ordinary differential equations (ODEs), written symbolically as

$$\dot{T} \simeq -V, \tag{1a}$$

$$\dot{V} \simeq T. \tag{1b}$$

https://doi.org/10.5194/cp-2021-136
Preprint. Discussion started: 14 October 2021

Climate of the Past Discussions
Open Access
EGU

Here T stands for global temperature and V for global ice volume, while Eq. (1a) is an EBM and Eq. (1b) is an ice-sheet model (ISM). The '$\simeq$' symbol stands for a binary relation of rough proportionality and is intended to neglect the details of the equation's right-hand side (RHS). The EBM represents the well-known ice-albedo feedback used by both Budyko (1969) and Sellers (1969), while the ISM relies on the precipitation-temperature feedback postulated by KCG and used also by Ghil and Le Treut (1981), who coined the term.

The latter feedback can be better understood by writing

$$\dot{V} \simeq p, \tag{2a}$$

$$p \simeq p_{\mathrm{ac}} - p_{\mathrm{ab}}, \tag{2b}$$

$$p_{\mathrm{ac}} \simeq T. \tag{2c}$$

Here p is net precipitation on the single ice sheet of the globally integrated model, given by the difference in Eq. (2b) between the accumulation p_{ac} and the ablation p_{ab} (KCG).

As first observed by George C. Simpson — the meteorologist of Robert F. Scott's *Terra Nova* expedition to the Antarctica in 1910–1912 and later the longest serving Director of the U.K. Meteorological Office — warmer winters have more snow and hence, at least in central Antarctica, the increase of p_{ac} with T exceeds the more obvious increase of p_{ab} with T. Hence $p \simeq T$ and we have derived therewith Eq. (1b), $V \simeq p \simeq T$. For more recent studies of the precipitation-temperature feedback, see Tziperman and Gildor (2002).

More generally, the presence of feedbacks of opposite sign in a system of two linear coupled ODEs

$$\dot{x} = y, \qquad \dot{y} = -x,$$

leads to an oscillation, with the solution given by two trigonometric functions in quadrature with each other, $x(t) = \sin(t)$, $y(t) = \cos(t) = \sin(t + \pi/2)$, and the trajectory describing a circle in the (x, y) phase plane, $x^2(t) + y^2(t) = 1$. In a nonlinear system, however — like the KCG model or any other climate oscillator mentioned so far — the possibility of an oscillation, as indicated by the system (1), is actually realized in the explicit, full set of equations only for certain parameter values and not for others.

This can be understood by considering the so-called normal form of a *Hopf bifurcation*, which leads from a stable steady state, called a fixed point in dynamical systems theory, to a stable oscillatory solution, called a limit cycle. The easiest way to see this transition is by writing the normal form in polar coordinates, as in Arnol'd (2012) and in Ghil and Childress (1987, Sec. 12.2), namely,

$$\dot{z} = (\mu + \imath\omega)z + c(z\bar{z})z. \tag{3}$$

Here $z = x + \imath y$ is complex, with $\imath = \sqrt{-1}$ the imaginary unit, while μ is a real bifurcation parameter, and c, ω are real and nonzero. Note that the KCG model per se is not in the normal form above and we will discuss its bifurcation parameter μ_* in the next subsection.

A very natural transformation of variables,

$$\rho = z\bar{z} > 0, \quad z = \rho^{1/2} \exp(\imath\theta) \tag{4}$$

https://doi.org/10.5194/cp-2021-136
Preprint. Discussion started: 14 October 2021

Climate of the Past Discussions
Open Access
EGU

leads from the complex ODE (3) to the system of two real and decoupled ODEs,

$$\dot{\rho} = 2\rho(\mu + c\rho), \tag{5a}$$

$$\dot{\theta} = \omega. \tag{5b}$$

Equation (5b) simply provides an angular rotation around the origin $\rho = 0 = x = y$, since the complex exponential in Eq. (4) is periodic with period 2π. Equation (5a) is quadratic in ρ and thus it can have two real roots, $\rho = \rho_0 = 0$ and $\rho = \rho_* = -\mu/c$. But ρ has to be positive and so, in the case in which $c < 0$, the only possible solution for $\mu < 0$ is the origin and it is stable, since $\rho(\mu + c\rho)$ is negative for $\rho > 0$, in this case; hence, ρ has to be monotonically decreasing, i.e., all the solutions of Eq. (5) spiral into the origin. The bifurcation from this stable steady state to a periodic solution with radius $\rho = \rho_*$ occurs as μ crosses 0, and this solution is stable, since now $\rho(\mu + c\rho) > 0$ for $0 < \rho < \rho_*$ and $\rho(\mu + c\rho) < 0$ for $\rho > \rho_*$, i.e. solutions will spiral out from inside the limit cycle and into it from the outside; see Ghil and Childress (1987, Fig. 12.7) for the so-called supercritical, or soft bifurcation case with $c < 0$.

2.2 Intrinsic Climate Oscillations and the Mid-Pleistocene Transition (MPT)

In this subsection, we present an argument for the role of intrinsic oscillations in the mid-Pleistocene transition (MPT). The argument starts with a further analysis of the Hopf bifurcation presented in the previous subsection. Such an analysis was carried out for the KCG model by Ghil and Tavantzis (1983).

Physically speaking, the presence or absence of the regular, purely periodic oscillations obtained by KCG and illustrated in Ghil and Childress (1987, Fig. 12.6) depends on whether $c \gtrless 0$ in Eq. (5a). The KCG model's bifurcation parameter is $\mu_* = c_T/c_L$, where c_T is the heat capacity in its EBM, while c_L is the "mass capacity" in its ISM (Ghil and Tavantzis, 1983). Large μ_* corresponds physically to a very small, possibly pre-Pleistocene ice cap (Ghil, 1984; Saltzman and Sutera, 1987). At these values of μ_*, the KCG model's isoclines and fixed points — the latter being given by the intersection of the former — are very different from those that are obtained for Quaternary-size ice sheets, for which c_L is comparable in value to c_T; see Ghil and Tavantzis (1983, Figs. 3–5). As μ_* decreases to $O(1)$, i.e., as we proceed from very small to more substantial ice sheets, the fixed point transfers its stability to a branch of periodic solutions, by a subcritical Hopf bifurcation (Källén et al., 1979; Ghil and Tavantzis, 1983); see also Ghil and Childress (1987, Figs. 12.8 and 12.9).

To clarify the simple physical concepts that underlie sub- and supercritical Hop bifurcations, let us consider a purely mechanical oscillator with mass m, a spring kx and a dashpot $\alpha\dot{x}$ (Landau and Lifshitz, 1960; Jordan and Smith, 1987),

$$m\ddot{x} = -\alpha(x)\dot{x} - k(x)x. \tag{6}$$

If k = const. and α = const., we have the simplest, linear setup, but we will be interested here in the nonlinear cases. Normalizing by the mass m and not changing notation otherwise, we get by rearranging terms and adding a periodic forcing

$$\ddot{x} + \alpha(x)\dot{x} + k(x)x = F\cos(\omega t). \tag{7}$$

Two classical nonlinear cases are those of the Duffing (1918) equation, in which $k(x) = x^2$ and α = const., and of the Van der Pol (1926) equation, in which k = const. and $\alpha(x) = \nu(x^2 - 1)$. The fully nonlinear case in which both the spring and the

https://doi.org/10.5194/cp-2021-136
Preprint. Discussion started: 14 October 2021


Climate of the Past Discussions

damping are nonlinear, with $k(x) = x^2$ and $\alpha(x) = \nu(x^2 - 1)$, is known as the Van der Pol–Duffing oscillator (e.g., Jackson, 1991; Pierini et al., 2018). Note that all three types of nonlinear oscillators can exhibit chaotic behavior even in the presence of simply periodic forcing (e.g., Guckenheimer and Holmes, 1983; Pierini et al., 2018, and references therein). The idea of using such simple, classical oscillators in modeling Quaternary glaciation cycles goes back to Saltzman et al. (1981).

Jordan and Smith (1987, Sec. 5.6) discuss specifically the case of a soft and a hard spring for a generalized Duffing equation, with $k(x) = k_0 + \epsilon h(x)$, where $0 < \epsilon \ll 1$, $h(-x) = h(x), h' \geq 0$, and $h'' > 0$. A spring is soft if it is sublinear, $\epsilon < 0$, and hard if it is superlinear, $\epsilon > 0$; see their Eq. (5.37) and Figs. 5.4(a,b), with $h(x) = x^2$. The supercritical Hopf bifurcation corresponds to a soft, sublinear spring in which the oscillations in the position x of the mass m increase gradually in amplitude as the spring constant k_0 increases past a critical value k_*, while the subcritical case corresponds to a hard, superlinear spring, where the oscillations in x jump suddenly from zero amplitude to a finite amplitude as the spring constant k_0 crosses the value k_*.

There is a clear-cut analogy with the mid-Pleistocene transition, occurring at roughly 0.8 Myr b2k, at which small-amplitude climate variability with a dominant periodicity near 40 kyr becomes larger, dominated by a periodicity that is close to 100 kyr, as well as being more irregular (e.g., Huybers, 2009; Rousseau et al., 2021). A fair number of distinct dynamical theories for this transition have been formulated (e.g., Ghil, 1994; Crucifix, 2012; Ashwin and Ditlevsen, 2015; Daruka and Ditlevsen, 2016; Ditlevsen and Ashwin, 2018). A rather obvious one is that a Hopf bifurcation occurs at that point, which leads to a more vigorous response to the multi-periodic orbital forcing; thus, the latter does not need to change in the least in order to explain the observed phenomena. In Saltzman and Sutera (1987), there is only a comment on the likely role of a Hopf bifurcation in the transition, but their Fig. 3 suggests that, in their model, such a bifurcation would have to be of the supercritical type, and lead to a fairly gradual transition.

To the contrary, the subcritical Hopf bifurcation of the KCG and Ghil and Le Treut (1981) oscillators would have to lead to a more abrupt transition, as suggested by Ghil (1984). The existing δ^{18}O and δ^{13}C records might or might not have sufficient resolution back in time up to 1.2 Ma to settle this question about the abruptness of the transition. In case some of them do, an objective test of suddenness, as proposed by Bagniewski et al. (2021) for the high-resolution NGRIP record (North Greenland Ice Core Project members, 2004), will have to be applied to such records.

3 TIME-DEPENDENT FORCING, NDSS AND RDSS

3.1 Orbital Forcing of a Climate Oscillator

We start this section by describing some fairly simple ways in which the orbital forcing might have interacted with intrinsic climate variability, thus helping to solve the mismatch between Figs. 3(a) and 3(b) in Section 1. To explore this possibility, Le Treut and Ghil (1983) used somewhat simplified insolation forcing, based on the calculations of Berger (1978), and applied it to a slightly modified version of the Ghil and Le Treut (1981) oscillator. These authors found that, as expected for a nonlinear oscillator, its internal frequency f_0 interacts with the forcing ones, $\{f_1, \ldots, f_5\}$, to produce both nonlinear resonance and combination tones (Landau and Lifshitz, 1960).

https://doi.org/10.5194/cp-2021-136
Preprint. Discussion started: 14 October 2021

Climate of the Past Discussions

Depending on parameter values, the periodicity $P_0 = 1/f_0$ of the Ghil and Le Treut (1981) oscillator is $P_0 \simeq 6$–7 kyr. The lines in the simplified insolation spectrum used by Le Treut and Ghil (1983) had the periodicities

$$P_1 = 19 \text{ kyr},\ P_2 = 23 \text{ kyr},\ P_3 = 41 \text{ kyr},\ P_4 = 100 \text{ kyr, and } P_5 = 400 \text{ kyr}; \tag{8}$$

these periodicities correspond to the two precessional ones, the obliquity one, and two eccentricity ones. The actual celestial mechanics calculations that Berger (1978) based his insolation calculations on have been substantially updated since (e.g., Varadi et al., 2003; Fienga et al., 2015). But these advances have not modified much the spectrum of the planetary-orbit solutions over the 2.6 Myr of the Quaternary, a rather short interval in celestial-mechanics terms.

The results of the Le Treut and Ghil (1983) model on the evolution of the primary climate variables T and V were converted to δ^{18}O values in simulated isotopic records of marine-sediment and ice cores by Le Treut et al. (1988); the spectra of the latter are plotted in Fig. 4. The values on the abscissa of Fig. 4(a) are values of the logarithm of frequency, while those in Fig. 4(b) are values of the frequency itself; the values on the ordinate of both panels are powers of 10. One refers to such figures as being in (a) log-log coordinates vs. (b) log-linear coordinates for short.

Aside from the spectral features noted in the figure caption and discussed in greater detail by Ghil (1994), it is important to realize (i) that the large continuous background in Fig. 4(a) is purely of deterministically chaotic origin, since there is no stochastic element whatsoever in the Le Treut and Ghil (1983) model or in its forcing; and (ii) that the dominant peak at 109 kyr is not directly forced by the $f_4 = 1/100$ (kyr)$^{-1}$ ecentricity line but rather it is due to the difference tone between the two precessional frequencies, f_1 and f_2. Finally, it is the nonlinear, broad resonance of the model's f_0 frequency with the quasi-periodic forcing that produces the bump in the spectrum of Fig. 4(a) to the right of the orbital frequencies.

In returning to the "fundamental question #2" in **Box 1**, one must recall that — apart from deterministic chaos à la Lorenz (1963), as obtained by H. Le Treut and colleagues (Le Treut and Ghil, 1983; Le Treut et al., 1988) and shown here in Fig. 4(a) — stochastic contributions à la Hasselmann (1976) to the continuous part of the paleoclimatic spectrum must also play an important role. In fact, the theory of random dynamical systems touched upon in the next subsection provides an excellent framework for a "grand unification" of these two complementary points of view (Ghil, 2014, 2019). In the paleoclimatic context, Ditlevsen et al. (2020) have suggested that, aside from red-noise processes, dating uncertainties in the proxy records from which the spectra are derived may contribute, in all likelihood, to this background; see also Boers et al. (2017a, b).

3.2 Basic Facts of NDS and RDS Life

The highly preliminary results on interaction between external forcing and internal variability summarized in Sec. 3.1 encourage us to pursue in a more systematic way the interaction between orbital forcing and intrinsic climatic variability that may have contributed to generate the rich paleoclimate spectrum on Quaternary and longer time scales (e.g., Westerhold et al., 2020). In fact, several research groups in the climate sciences have carried out during the past two decades an important extension of the dynamical-systems and model hierarchy framework presented by Ghil and Childress (1987) and by Ghil (2001), from deterministically autonomous to nonautonomous and random dynamical systems (NDSs and RDSs: e.g., Ghil et al., 2008; Chekroun et al., 2011; Bódai and Tél, 2012).

https://doi.org/10.5194/cp-2021-136
Preprint. Discussion started: 14 October 2021

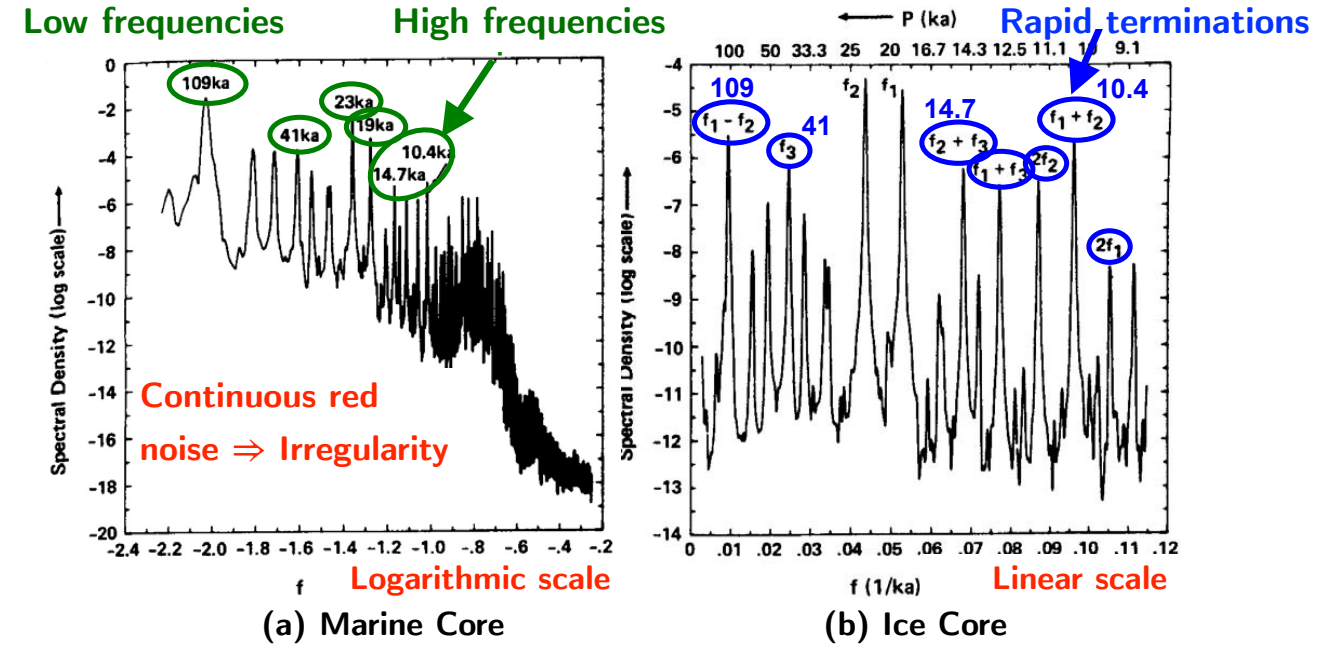

Figure 4. Power spectra of simulated (a) deep-sea and (b) ice core records for the forced climate oscillator of Le Treut and Ghil (1983) with idealized orbital forcing. Panel (a) is in log-log coordinates and clearly shows a dominant peak at 109 kyr and a very large amount of variance in the continuous spectrum, which has a roughly -2 power law slope. The orbital peaks at $P_1 = 19$ kyr, $P_2 = 23$ kyr and $P_3 = 41$ kyr are also present along with peaks at 14.7 kyr and 10.4 kyr, which correspond to the sum tones $f_2 + f_3$ and $f_1 + f_2$, respectively. Panel (b) is in log-linear coordinates and shows additional harmonics and sum tones, as well as the difference tone $f_1 - f_2$, which corresponds to the dominant peak at 109 kyr. After Le Treut et al. (1988) with permision from Wiley.

On the road to including deterministically time-dependent, as well as random effects, one needs to realize first that the climate system — as well as any of its subsystems, and on any time scale — is not closed: it exchanges energy, mass and momentum with its surroundings, whether other subsystems or the interplanetary space and the solid earth. The typical applications of dynamical systems theory to climate variability until not so long ago have only taken into account exchanges that are constant in time, thus keeping the model — whether governed by ordinary, partial or other differential equations — autonomous; i.e., the models had coefficients and forcings that were constant in time.

Alternatively, the external forcing or the parameters were assumed to change either much more slowly than a model's internal variability, so that the changes could be assumed to be quasi-adiabatic, or much faster, so that they could be approximated by stochastic processes. Some of these issues are covered in much greater detail by Ghil and Lucarini (2020, Sec. III.G). The key concepts and tools of NDSs and RDSs go beyond such approaches that rely in an essential way on a scale separation between the characteristic times of the forcing and the internal variability of a given system; such a separation is rarely, if ever, actually present in the climate sciences.

https://doi.org/10.5194/cp-2021-136
Preprint. Discussion started: 14 October 2021


Climate of the Past Discussions
Open Access
EGU

The presentation of the key NDS and RDS concepts and tools in this subsection is aimed at as large a readership as possible and it follows Ghil (2014). Slightly more in-depth, but still fairly expository presentations can be found in Crauel and Kloeden (2015) and in Caraballo and Han (2017). Readers who are less interested in this mathematical framework — which allows a truly thorough understanding of the way that orbital forcing interacts with intrinsic climate variability on Quaternary time scales — may skip at a first reading the remainder of this section and continue with Section 4.

Autonomous and nonautonomous systems. Succinctly, one can write an autonomous system as

$$\dot{\mathbf{X}} = \mathbf{F}(\mathbf{X}; \mu), \tag{9}$$

where $\mathbf{X}$ stands for any state vector or climate field. While $\mathbf{F}$ is a smooth function of $\mathbf{X}$ and of the parameter μ, it does not depend explicitly on time. This autonomous character of Eq. (9) greatly facilitates the analysis of its solutions' properties.

For instance, two distinct trajectories, $\mathbf{X}_1(t)$ and $\mathbf{X}_2(t)$, of a well-behaved, smooth autonomous system cannot intersect — i.e., they cannot pass through the same point in phase space — because of the uniqueness of solutions. This property helps one draw the phase portrait of an autonomous system, as does the fact that we only need to consider the behavior of solutions $\mathbf{X}(t)$ as time t tends to $+\infty$. The sets of points so obtained are — possibly multiple — equilibria, periodic and quasi-periodic solutions, and chaotic sets. In the language of dynamical systems theory, these are called, respectively: *fixed points, limit cycles, tori,* and *strange attractors.*

We know only too well, however, that the seasonal cycle plays a key role in climate variability on interannual time scales, while orbital forcing is crucial on the Quaternary time scales of many millennia. And, more recently, it has become obvious that anthropogenic forcing is of utmost importance on the interdecadal time scales in-between.

How can one take into account these types of time-dependent forcings, and analyze the nonautonomous systems that they lead us to formulate? One writes succinctly such a system as

$$\dot{\mathbf{X}} = \mathbf{F}(\mathbf{X}, t; \mu). \tag{10}$$

In Eq. (10), the dependence of $\mathbf{F}$ on t may be periodic, $\mathbf{F}(\mathbf{X}, t+P) = \mathbf{F}(\mathbf{X}, t)$, as in various El Niño–Southern Oscillation (ENSO) models, where the period $P = 12$ months, or monotone, $\mathbf{F}(\mathbf{X}, t+\tau) \geq \mathbf{F}(\mathbf{X}, t)$, as in studying scenarios of anthropogenic climate forcing. An even more general situation includes time dependence in one or more parameters $\{\mu_1, \ldots, \mu_p\}$.

To illustrate the fundamental distinction between an autonomous system like Eq. (9) and a nonautonomous one like Eq. (10), consider the simple scalar version of these two equations:

$$\dot{X} = -\beta X, \qquad \text{and} \tag{11a}$$

$$\dot{X} = -\beta X + \gamma t, \tag{11b}$$

respectively. We assume that both systems are dissipative, i.e. $\beta > 0$, and that the forcing is monotone increasing, $\gamma \geq 0$, as would be the case for anthropogenic forcing in the industrial era. Lorenz (1963) pointed out the key role of dissipativity in giving rise to strange, but attracting solution behavior, while Ghil and Childress (1987) emphasized its importance and pervasive character in climate dynamics. Clearly the only attractor for the solutions of Eq. (11a), given any initial point $X(0) = X_0$, is the stable fixed point $X_* = 0$, attained as $t \to +\infty$.

https://doi.org/10.5194/cp-2021-136
Preprint. Discussion started: 14 October 2021


Climate of the Past Discussions
Open Access
EGU

In the case of Eq. (11b), though, this forward-in-time approach yields blow-up as $t \to +\infty$, for any initial point. To make sense of what happens in the case of time-dependent forcing, one introduces instead the *pullback approach*, in which solutions are allowed to still depend on the time t at which we observe them, but also on a time s from which the solution is started, with $X(s) = X_0$ and $s \ll t$. With this little change of approach, one can easily verify that

$$|X(s,t;X_0) - \mathcal{A}_t| \to 0 \quad \text{as} \quad s \to -\infty, \tag{12}$$

for all t and X_0, where $\mathcal{A}_t = (\gamma/\beta)(t - 1/\beta)$. We obtain therewith, in this pullback sense, the intuitively obvious result that the solutions, if we start them far enough in the past, all approach the family of attracting sets $\mathcal{A}_t$; this family follows the forcing γt and it thus has a linear growth in time t. Hence, the fixed point X_* of Eq. (11b) is, in fact, a moving target and it is given by $X_* = \gamma t/\beta$. Due to the system's inertia, the set $\mathcal{A}_t$ that is approached by the trajectories lags this time-dependent fixed point by a constant offset of γ/β^2.

Pullback attractor (PBA). Formally, the indexed family $\mathscr{A}$ of all pullback attracting sets $\mathcal{A}_t$

$$\mathscr{A} = \{\mathcal{A}_t\}_{t\in\mathbb{R}} \tag{13}$$

is termed the *pullback attractor* (PBA) of the NDS if the following two conditions are fulfilled:

(i) each snapshot $\mathcal{A}_t$ is compact and the family of snapshots $\{\mathcal{A}(t)\}_{t\in R}$ is invariant with respect to the dynamics

$$X(t,s;X_0) \in \mathcal{A}_t \quad \forall s \le t \text{ and } X_0 \in A_s; \text{ and} \tag{14}$$

(ii) the pullback attraction occurs for all times:

$$\lim_{s\to-\infty} |X(t,s;X_0) - \mathcal{A}_t| \to 0 \quad \forall t. \tag{15}$$

To further improve the reader's intuition for PBAs, we provide a second illustrative example here. A system defined in polar coordinates by

$$\dot{\rho} = \alpha(\mu - \rho), \quad \dot{\phi} = \omega, \quad \text{with } \rho, \mu \in \mathbb{R}^+ \text{ and } \phi \in \mathbb{R}/2\pi, \tag{16}$$

can easily be seen to exhibit a limit cycle in the (x,y)-plane with $(x = \rho\cos\phi, y = \rho\sin\phi)$. An initial deviation of ρ from μ will decay exponentially and the system converges to an oscillation of radius μ with the angular velocity ω. Here, we transform this autonomous dynamical system into a nonautonomous one by modulating the target radius μ with a sinusoidal forcing

$$\mu \to \mu(t) = \mu + \beta\sin(\nu t), \tag{17}$$

where the modulation is moderate, so as to guarantee that $\mu + \beta\sin(\nu t) > 0$ for all t.

Since the dynamics of the phase ϕ and of the radius ρ are decoupled, the corresponding equations can be solved and analyzed separately. While the temporal development of the phase is trivial, the pullback invariant attracting set of the radius for the initial

https://doi.org/10.5194/cp-2021-136
Preprint. Discussion started: 14 October 2021

Climate of the Past Discussions
Open Access
EGU

condition $\rho(s) = \rho_0$ is given by

$$\mathcal{A}^{(\rho)}(t;\rho_0) = \lim_{s\to-\infty} \rho(t,s;\rho_0) = \alpha\beta\sin(\nu t + \vartheta) + \mu, \quad \text{with} \tag{18a}$$

$$\vartheta = \arctan(-\nu/\alpha), \tag{18b}$$

as shown in Appendix A. Note that, in the limit $s \to -\infty$, the dependence on the initial value ρ_0 vanishes and the attracting set $\mathcal{A}_t^{(\rho)}$ performs an oscillation of the same frequency as the forcing. It lags the phase of the time-dependent fixed point by the constant ϑ, while its amplitude is amplified by the factor α. Since ρ is restricted to positive values, this solution requires $\alpha\beta < \mu$.

The PBA with respect to the coordinate ρ is comprised of the family of all the sets $\mathcal{A}_t^{(\rho)}$ as defined in (18) and thus reads

$$\mathscr{A}^{(\rho)} = \{\alpha\beta\sin(\nu t + \vartheta) + \mu\}_{t\in\mathbb{R}}. \tag{19}$$

Since the pullback limit for the phase ϕ does not exist, no constraints on it other than $\phi \in [0, 2\pi)$ are imposed by the dynamics. Hence, for the system (16) comprised of radius and phase, we find that

$$\lim_{t_0\to-\infty} d_{\mathrm{H}}\Big(\big(\rho(t;t_0,\rho_0),\phi(t;t_0,\phi_0)\big), \underbrace{\{\big(\alpha\beta\sin(\nu t+\vartheta)+\mu,\varphi\big) : \varphi\in[0,2\pi)\}}_{\mathcal{A}_t}\Big) = 0, \tag{20}$$

where d_{H} denotes the Hausdorff semi-distance. The pullback attracting sets $\mathcal{A}_t$ at time t are circles in the (x,y)-plane with oscillating radius, and the system's PBA is given by the family of these circles

$$\mathscr{A} = \{\big(\alpha\beta\sin(\nu t+\vartheta)+\mu,\varphi\big) : \varphi\in[0,2\pi)\}_{t\in\mathbb{R}}. \tag{21}$$

Figure 5 shows trajectories of the system starting from different points in the past. In panel (a) the trajectories are depicted in the three-dimensional (3-D) space spanned by the two cartesian coordinates (x,y) and the time t, where the usual transformation from polar to cartesian coordinates was applied. The shaded surface in this panel represents the PBA of the system. Panel (b) shows a heat map (Wilkinson and Friendly, 2009) that approximates a portion of the PBA's invariant measure projected onto the (x,y)-plane. For a clean definition of such a measure in NDSs and RDSs, please see Caraballo and Han (2017); Chekroun et al. (2011); Crauel and Kloeden (2015) or Ghil et al. (2008). Essentially, the heat map here counts the number of times that 100 trajectories integrated from $t = -200$ to $t = 200$ with randomized initial conditions like the ones shown in panel (a) cross small pixels in the (x,y)-plane.

Note that the structure of the system's trajectories depends on the ratio ω/ν and three different cases must be distinguished. If the radius is modulated with the same frequency as the oscillation itself, i.e. $\omega = \nu$, after one period the system practically repeats its orbit. More precisely, the radius of the oscillation does differ from one "roundtrip" to the next, but this difference tends to zero as $\rho(t)$ asymptotically approaches $\mathcal{A}_t^{(\rho)}$. If ω and ν are rationally related, $m\omega = n\nu$ with $n,m\in\mathbb{N}$, then the same quasi-repetition of the orbit occurs after n periods of the radial modulation and m periods of the system's oscillation. Such a trajectory will appear as an n-fold quasi-closed loop. Finally, if $\omega/\nu \notin \mathbf{Z}$, then the trajectory does not repeat itself but

https://doi.org/10.5194/cp-2021-136
Preprint. Discussion started: 14 October 2021

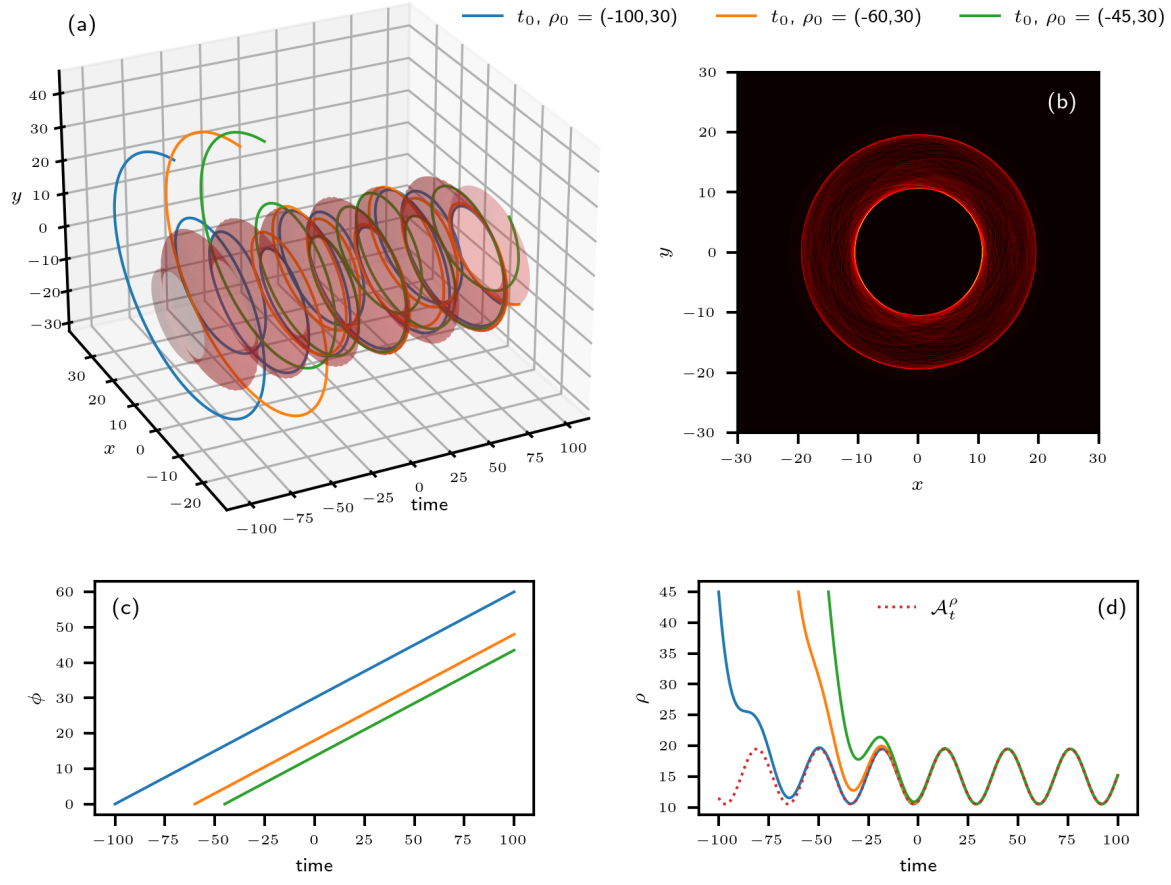

Figure 5. Trajectories and PBA of the system defined by Eqs. (16) and (17). (a) Trajectories $(\rho(t), \phi(t))$ of the system starting from different times in the past in the 3-D space spanned by the two cartesian coordinates (x, y) and time t; the system's PBA lies on the red-shaded surface. (b) Heat map of the trajectories projected onto the (x, y)-plane. A video of the heat map filling up, as more and more trajectories with different initial conditions are added, is provided in the Supplementary Material to this article. The heat map here is a snapshot of the video taken at time $t = 0.20$; see details in the Video supplement. (c) Temporal evolution of the phase. (d) Temporal evolution of the radius (solid colors) together with its PBA (dotted red).

https://doi.org/10.5194/cp-2021-136
Preprint. Discussion started: 14 October 2021


Climate of the Past Discussions
Open Access
EGU

instead covers densely the annular disc $\mathcal{D} = \{(\rho, \phi) : \rho \in [\mu - \alpha\beta, \mu + \alpha\beta]$ and $\phi \in [0, 2\pi)\}$. The trivial evolution of the phase is depicted in panel (c), while the trajectories of $\rho(t)$ and their convergence to $\mathcal{A}_t^{(\rho)}$ are shown in panel (d).

Random attractor. Let us return now to the more general, nonlinear case of Eq. (10) and add not only deterministic time dependence $\mathbf{F}(\mathbf{X}, t)$, but also random forcing,

$$\mathrm{d}\mathbf{X} = \mathbf{F}(\mathbf{X}, t)\mathrm{d}t + \mathbf{G}(\mathbf{X})\mathrm{d}\eta, \tag{22}$$

where $\eta = \eta(t, \omega)$ represents a Wiener process — with $\mathrm{d}\eta$ commonly referred to as "white noise" — and ω labels the particular realization of this random process. When $\mathbf{G} =$ const. the noise is additive, while for $\partial\mathbf{G}/\partial\mathbf{X} \neq 0$ we speak of multiplicative noise. The distinction between $\mathrm{d}t$ and $\mathrm{d}\eta$ in the stochastic differential equation (22) is necessary since, roughly speaking and following the Einstein (1905) paper on Brownian motion, it is the variance of a Wiener process that is proportional to time and thus $\mathrm{d}\eta \propto (\mathrm{d}t)^{1/2}$. In Eq. (22), we dropped the dependence on a parameter μ for the sake of simplicity.

The noise processes may include "weather" and volcanic eruptions when $\mathbf{X}(t)$ is "climate," thus generalizing the linear model of Hasselmann (1976), or cloud processes when we are dealing with the weather itself: one person's signal is another person's noise, as the saying goes. In the case of random forcing, the concepts introduced by the simple example of Eq. (11b) above can be illustrated by the *random attractor* $\mathscr{A}(\omega)$ in Fig. 6.

Chekroun et al. (2011) studied a specific case of such a random attractor for the paradigmatic, climate-related Lorenz (1963) convection model. The authors introduced multiplicative noise into each of the ODEs of the original, deterministically chaotic system, as shown below:

$$\mathrm{d}X = P_r(Y - X)\mathrm{d}t + \sigma X\mathrm{d}\eta, \tag{23a}$$

$$\mathrm{d}Y = (rX - Y - XZ)\mathrm{d}t + \sigma Y\mathrm{d}\eta, \tag{23b}$$

$$\mathrm{d}Z = (-bZ + XY)\mathrm{d}t + \sigma Z\mathrm{d}\eta; \tag{23c}$$

here $r = 28$, $P_r = 10$, $b = 8/3$ are the standard parameter values for chaotic behavior in the absence of noise, and σ is a constant variance of the Wiener process that is not necessarily small. The well-known strange attractor of the deterministic case is replaced by the Lorenz model's random attractor, dubbed LORA by the authors. Four *snapshots* $\mathcal{A}_t(\omega)$ of LORA are plotted in Fig. 7 and a video of its evolution in time $\mathscr{A}(\omega) = \{\mathcal{A}_t(\omega)\}_{t\in\mathbb{R}}$ is available as Supplementary Material in Chekroun et al. (2011) at https://doi.org/10.1016/j.physd.2011.06.0052011.06.005.

Charó et al. (2021) have further analyzed the striking effects of the noise on the nonlinear dynamics that are visible in Fig. 7 here and in the video of Chekroun et al. (2011), and gathered further insights into the abrupt changes of the snapshots' topology at critical points in time. These remarkable changes suggest the possibility of random processes giving rise to qualitative jumps in paleoclimatic variability, such as the MPT.

3.3 Application to Dansgaard-Oeschger (D-O) events

Before discussing conceptual glacial cycle models, we take a little detour and introduce a simpler — yet interesting and, at the same time, highly instructive — application of NDS theory to another important climate phenomenon. During past glacial

https://doi.org/10.5194/cp-2021-136
Preprint. Discussion started: 14 October 2021

Climate of the Past Discussions
Open Access
EGU

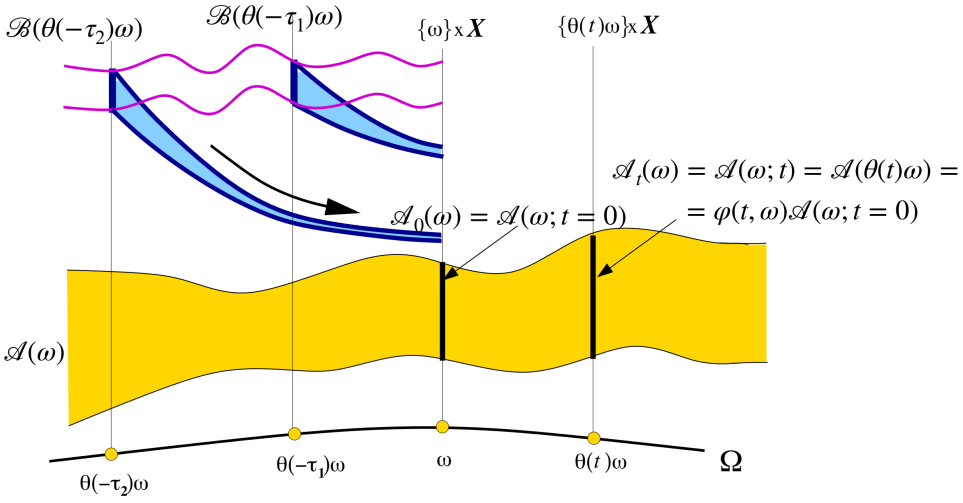

Figure 6. Schematic diagram of a random attractor $\mathscr{A}(\omega)$ and of the pullback attraction to it; here ω labels the particular realization of the random process $\theta(t)\omega$ that drives the system. We illustrate the evolution in time t of the random process $\theta(t)\omega$ (light solid black line at the bottom); the random attractor $\mathscr{A}(\omega)$ itself (yellow band in the middle), with the *snapshots* $\mathcal{A}_0(\omega) = \mathcal{A}(\omega;t=0))$ and $\mathcal{A}(\omega;t)$ (the two vertical sections, heavy solid); and the flow of an arbitrary compact set $\mathcal{B}$ from "pullback times" $t=-\tau_2$ and $t=-\tau_1$ onto the attractor (heavy blue arrows). See Ghil et al. (2008, Appendix A) for the requisite properties of the random process $\theta(t)\omega$ that drives the RDS (22). Reproduced from Ghil et al. (2008) with permission from Elsevier.

periods, Greenland experienced a series of sudden decadal-scale warming events that left a clear trace in ice core records (Dansgaard et al., 1993). These so-called D-O events were followed by intervals of steady moderate cooling, before a short phase of enhanced cooling brought the temperatures back to their pre-event levels (e.g., Rasmussen et al., 2014). This pattern is very clearly apparent in NGRIP δ^{18}O records (North Greenland Ice Core Project members, 2004) and it can be mimicked qualitatively by the fast component of a FitzHugh-Nagumo (FHN) model (FitzHugh, 1961; Nagumo et al., 1962), as pointed out by Mitsui and Crucifix (2017), among others; see also Kwasniok (2013); Rial and Yang (2007).

The FitzHugh-Nagumo (FHN) model of fast-slow oscillations. The FHN model consists of two coupled ODEs that govern behavior alternating between slow evolutions and fast transitions. Typically, the time scales of the two variables are separated by introducing the parameters τ_x and τ_y, with $x(t)$ being the slow component and $y(t)$ the fast one:

$$\dot{x} = \frac{1}{\tau_x}(y-\gamma), \tag{24a}$$

$$\dot{y} = \frac{1}{\tau_y}[\alpha(y-y^3)-x]. \tag{24b}$$

https://doi.org/10.5194/cp-2021-136
Preprint. Discussion started: 14 October 2021

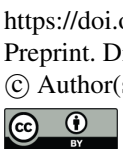

Climate of the Past Discussions
Open Access
EGU

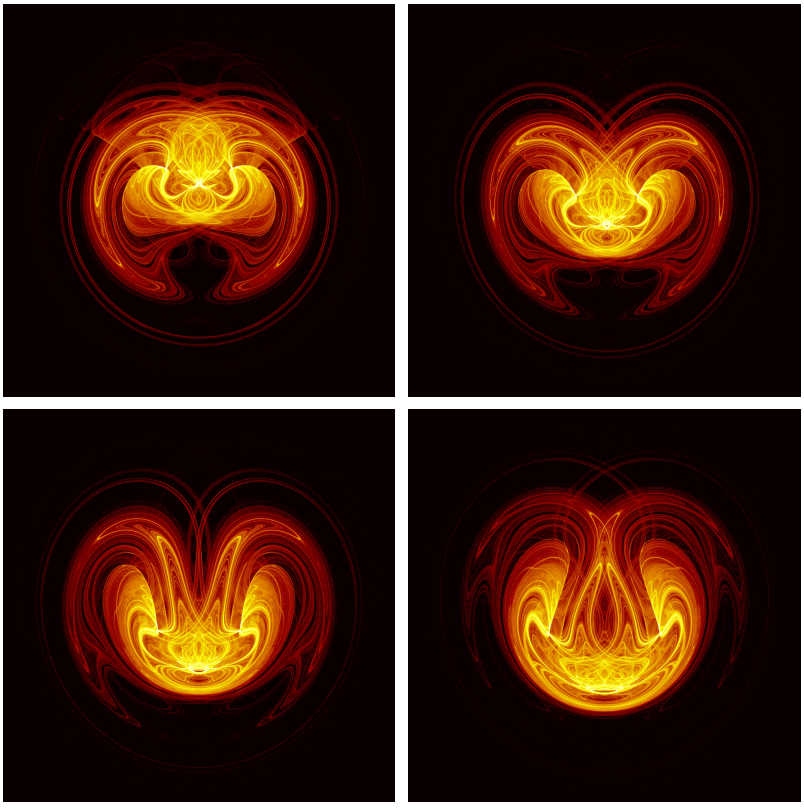

Figure 7. Heat maps of the time-dependent invariant measure $\nu_t(\omega)$ supported on four snapshots $\mathscr{A}_t(\omega)$ of LORA. The values of the parameters r, s and b are the classical ones, while the variance of the noise $\sigma = 0.5$. The color bar is on a log-scale and it quantifies the probability of landing in a particular region of phase space; shown is a projection of the 3-D phase space (X, Y, Z) onto the (X, Z)-plane. Note the complex, interlaced filament structures between highly populated regions (in yellow) and moderately populated ones (in red). Reproduced from Ghil et al. (2008) with permission from Elsevier.

In order to develop an understanding for the way that such a model can simulate the rapid D-O warmings, followed by slow coolings, we shall discuss its autonomous behavior, for time-independent γ, first. Next, we shall give a physical meaning to the variables in the climate context and introduce time-dependent forcing exerted by a background state via $\gamma = \gamma(t)$.

Consider the case of large time scale separation

$$\tau_x >> \tau_y. \tag{25}$$

This choice guarantees that the fast y-component adjusts adiabatically to quasi-static changes of the slow x-component. The time derivative of $y(t)$, as shown in Fig. 8(a), exhibits either three real roots or a single one, depending on the value of $x(t)$, which shifts the graph of the cubic polynomial $P_3(x, y) = \alpha(y - y^3) - x$ globally upwards or downwards. Of the three potential roots, the outer two are stable fixed points for $y(t)$ at a fixed value of x, while the inner one is unstable. Note that the two stable fixed points are always located either left or right of the local minimum or maximum of $P_3(x, y)$, respectively. Accordingly,

https://doi.org/10.5194/cp-2021-136
Preprint. Discussion started: 14 October 2021

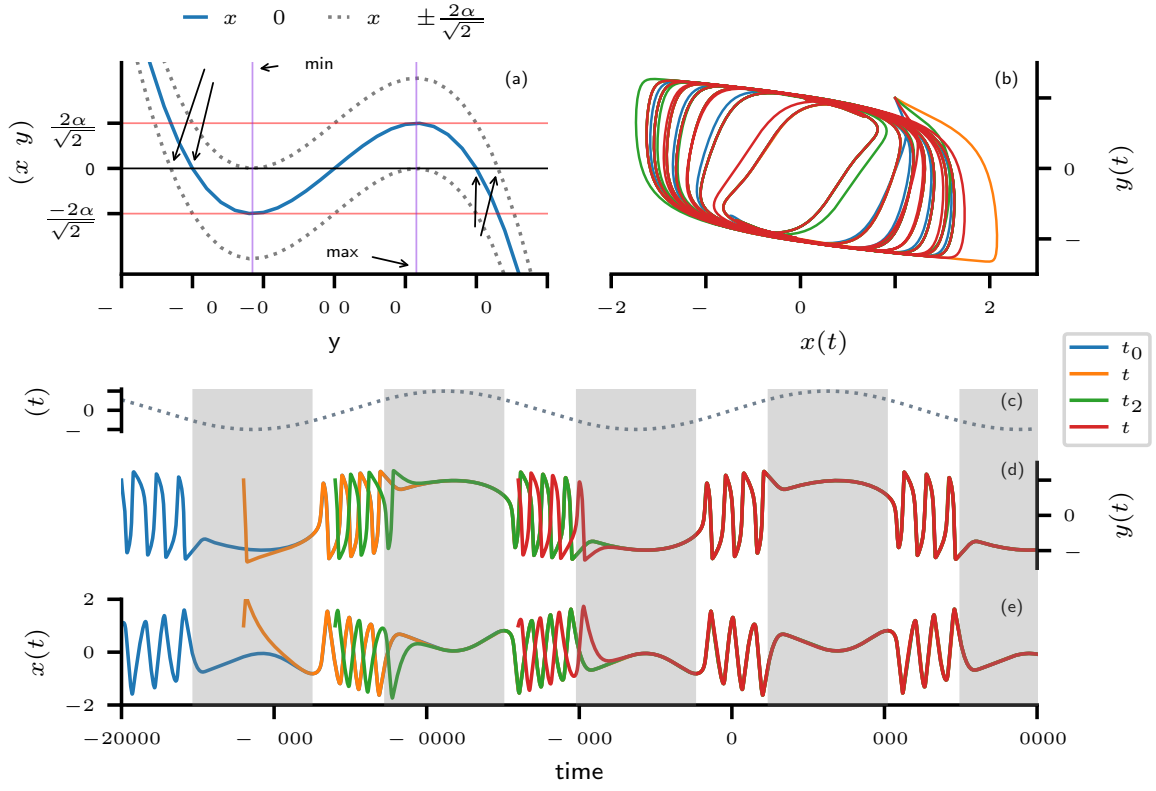

Figure 8. FitzHugh-Nagumo (FHN) model with time scales $\tau_f = 2000$, $\tau_x = 100$, $\tau_y = 60$, and $\alpha = 2$. (a) The cubic term of the fast derivative $P_3(x, y)$ as a function of y for $x = 0$ (solid blue line); dashed lines indicate the same function with $x = \pm 2\alpha/\sqrt{27}$. (b) Trajectories of the nonautonomous model, with $\gamma(t) = \sin(t/\tau_f)$, and starting at the times $\{t_0 = -20$ kyr, $t_1 = -16$ kyr, $t_2 = -13$ kyr, $t_3 = -7$ kyr$\}$ in the (x, y)-plane, using different colors for t_0, t_1, t_2 and t_3. (c) The time-dependent forcing $\gamma = \gamma(t)$. (d, e) The same trajectories as in (b), but plotted in time, as $y = y(t)$ and $x = x(t)$, respectively. ; in panels (c)–(e), the gray shading indicates intervals during which $|\gamma| > \sqrt{1/3}$ and the internal oscillation is suppressed.

we label them y_ℓ and y_r. Thus, the positions of the local extrema, namely $y_{\min} = -\sqrt{1/3}$ and $y_{\max} = \sqrt{1/3}$, provide an upper and a lower bound for the left and right stable fixed point, respectively.

Given the large time scale separation, the y-component will be close to either one of the two stable fixed points for a given x; hence, $y(t)$ must be outside the interval spanned by the two local extrema: $y(t) \notin (-\sqrt{1/3}, \sqrt{1/3})$. In the overall evolution of the solution, though, the stable fixed point that momentarily attracts $y(t)$ is destabilized by a slow adjustment of $x(t)$, and a fast transition to the neighborhood of the opposite stable fixed point ensues. This switches the sign of $\dot{x}(t)$ and the slow adjustment of $x(t)$ now happens in the opposite direction. In the (x, y)-plane, this behavior manifests itself as a stable limit cycle. However, any value $|\gamma| > \sqrt{1/3}$ prevents $\dot{x}(t)$ from switching sign and therefore interrupts the cyclic destruction and

https://doi.org/10.5194/cp-2021-136
Preprint. Discussion started: 14 October 2021


Climate of the Past Discussions

revival of the opposite fixed points for $y(t)$. Instead, $|\gamma| > \sqrt{1/3}$ gives rise to a single stable fixed point for the entire system in the (x, y)-plane and, in this case, both variables relax towards this equilibrium.

In fact, in the autonomous setting, the system's qualitative behavior is ultimately controlled by the value of the parameter γ, which decides between internal oscillations along a limit cycle and relaxation towards a fixed point in the (x, y)-plane. This highly nonlinear, two-time behavior modifies somewhat the general appearance of stable limit cycles via Hopf bifurcation whose normal form, given by Eqs. (3–5), was discussed in Sec. 2.1.

Introducing a sinusoidal time dependence

$$\gamma \to \gamma(t) = \sin(t/\tau_{\mathrm{f}}) \tag{26}$$

into the slow equation (24a) makes the system nonautonomous, as discussed in general terms in Sec. 3.2, and it periodically switches the self-oscillatory behavior on and off. We consider here the case in which the external forcing $\gamma(t; \tau_{\mathrm{f}})$ varies slowly with respect to all internal dynamics, i.e.,

$$\tau_{\mathrm{f}} >> \tau_x >> \tau_y. \tag{27}$$

The trajectories plotted in Figs. 8(b)–(e) represent, in fact, the solutions of such a periodically forced FHN model starting at different points in the past on an arbitrary time axis. These trajectories illustrate the applicability of the pullback perspective suggested by Sec. 3.2 and Fig. 5 to the periodically forced FHN model. In contrast to the previous examples, an analytical solution is not available in this case. However, this small sample of numerically computed trajectories, together with the phenomenological discussion herein, is quite sufficient for an intuitive understanding of the system's pullback behavior.

Most strikingly, the trajectory t_1 that starts at $-16\,000$ during a nonoscillatory time interval is immediately synchronized to the trajectory t_0 that started even earlier, at $-20\,000$. The other two trajectories both start during intervals when internal oscillations are supported and maintain their individual phase throughout the oscillatory interval. It takes a breakdown of the limit cycles and attraction to a common stable fixed point for these trajectories to synchronize to the "older" trajectories. Here, synchronization means that they can visually no longer be distinguished; numerically, however, the distance between trajectories only tends to zero but never reaches it.

The model trajectories' behavior in the figure can be explained, in greater detail, as follows: whenever $|\gamma(t)| > \sqrt{1/3}$, all trajectories are attracted by a single point in the (x, y)-plane; hence — given the system's intrinsic dynamics being fast with respect to the forcing, cf. Eq. (27) — during a single nonoscillatory time interval, all trajectories are strongly bundled by the fixed point and can no longer be discriminated visually. This bundling guarantees that the distance between different trajectories becomes arbitrarily small after only a few nonoscillatory intervals. Furthermore, the system's fixed point during the nonoscillatory behavior is fully determined by $\gamma(t)$; therefore, at the end of such an interval, the system reenters the oscillatory regime always from the same location in the (x, y)-plane and, therewith, the trajectories very nearly repeat themselves. Qualitatively speaking, the PBA $\mathscr{A}$ — or, according to Eq. (14), the family of invariant snapshots $\{\mathcal{A}(t)\}_{t\in\mathbb{R}}$ — is an infinite repetition of the common trajectory structure that can be observed in Figs. 8(d,e) between 0 and 10 000.

An FHN model of the NGRIP record. Readers who are familiar with the NGRIP δ^{18}O record (North Greenland Ice Core Project members, 2004) might have realized already the resemblance between the proxy data and the fast component's trajec-

https://doi.org/10.5194/cp-2021-136
Preprint. Discussion started: 14 October 2021

Climate of the Past Discussions
Open Access
EGU

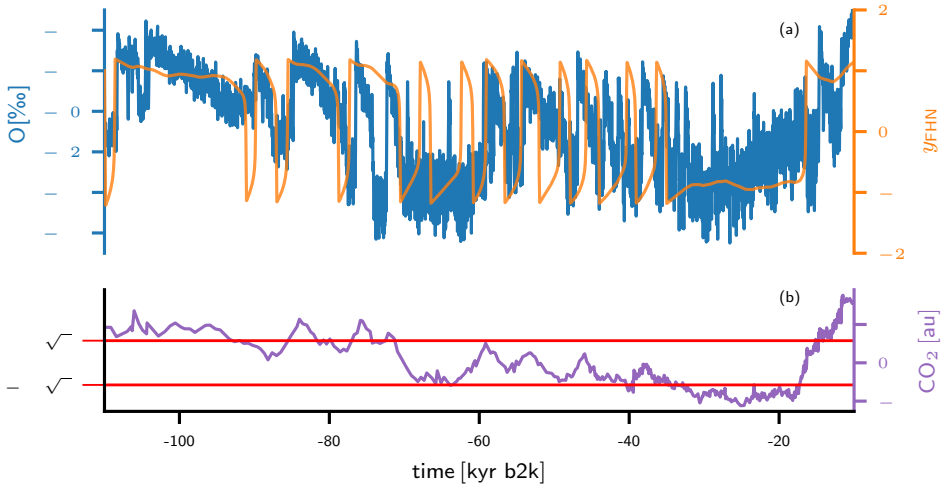

Figure 9. FHN model fit to the NGRIP δ^{18}O data. (a) Fast component $y_{\mathrm{FHN}}(t)$ of an FHN model forced with historical CO_2 concentrations (orange) together with the observed δ^{18}O record (blue) from the NGRIP ice core (Seierstad et al., 2014). (b) Rescaled atmospheric CO_2 concentrations from Antarctic ice cores in arbitrary units (au) (Bereiter et al., 2015); the horizontal red lines indicate the upper and lower bounds, $y_{\mathrm{min}} = -\sqrt{1/3}$ and $y_{\mathrm{max}} = \sqrt{1/3}$, of the free-oscillation regime.

tory of the periodically forced FHN model in Fig. 8(d). In particular, the prominent sawtooth pattern of the data is satisfactorily captured by the fast-slow dynamics of the model.

Figure 9 shows a trajectory of the FHN model for which the sinusoidal forcing used in Fig. 8 was replaced by a rescaled time series of atmospheric CO_2 concentrations retrieved from Antarctic ice cores (Bereiter et al., 2015):

$$\gamma(t) \propto \mathrm{CO}_2(t). \tag{28}$$

Is it remarkable how well this simple forcing brings the oscillatory intervals of the FHN model into agreement with the time intervals of the record that are dominated by D-O cycles, without any systematic tuning of the model parameters. Clearly, the CO_2-forced FHN model fails to reproduce the exact waiting times between D-O events. However, with these waiting times being at least in part stochastically determined (Ditlevsen et al., 2007), the purely deterministic FHN model is not meant to reproduce the exact pattern of D-O events. Vettoretti et al. (under review) have carried out a detailed study on the use of a CO_2-forced FHN model to simulate D-O variability.

In fact, Rousseau et al. (2021, Fig. 6) describe in detail a somewhat more complex, proxy record-based picture of the interaction between D-O event-rich episodes, Heinrich (1988) events, and longer-term cooling trends. It is quite possible that a simple model like the one in this section but including explicitly continental ice sheets could capture such a detailed picture.

In the present framework, the FHN model's fast variable $y(t)$ may be interpreted as the intensity of the Atlantic Meridional Overturning Circulation (AMOC), which switches between on and off states during self-oscillatory behavior; see, for instance,

https://doi.org/10.5194/cp-2021-136
Preprint. Discussion started: 14 October 2021

Climate of the Past Discussions
Open Access
EGU

The concepts and tools summarized in Sec. 3.2 could shed further light on several problems not quite yet solved concerning Quaternary glaciations and paleoclimate in general. A short and highly incomplete list of the interesting problems that might gain by such a treatment is the following:

1. What are the causes of the MPT and what is the part of intrinsic climate variability and that of the orbital forcing therein? See discussion in Sec. 2.2.
2. What causes the large continuous backgound of the observed spectrum: is it deterministic chaos, stochastic forcing or both? See discussion of Fig. 4.
3. Particularly complex problems are associated with Heinrich and D-O events and their modulation over longer time intervals by orbital forcing and other slow-acting changes in atmospheric composition, geology, ocean circulation, and so on. See, for instance, Rousseau et al. (2021, and references therein).
4. It is well established by now that a snowball mode occurred several times in Earth's geologic history, but we still know fairly little about how the planet got into, and especially out of, such a mode (e.g., Pierrehumbert,2004).

Box 2. Some open questions concerning Quaternary glaciations.

Henry et al. (2016), Ghil (1994, Table 5) and Ghil and Lucarini (2020, Table I). The slower x-variable that drives the transition between the on and off states of the AMOC may then be taken, for instance, as the waxing and waning of northern hemisphere ice sheets (e.g., Ghil et al., 1987), linked in turn to varying ice shelf extent (e.g., Boers et al., 2018).

The interaction between the fast variable and the slow one happens here in the presence of a climate forcing represented by CO_2 concentration. On the much slower time scales of Quaternary glaciations, an interplay between the CO_2 concentration and mean global temperature might also occur, as we shall see in the next section.

4 AN NDS FOR THE QUATERNARY GLACIATIONS

Apparently, it is Crucifix (2013) who first applied pullback ideas to the problems of Quaternary glaciations, independently of earlier work on the topic in the climate literature (Ghil et al., 2008; Chekroun et al., 2011; Bódai and Tél, 2012). His work concentrated mainly on the connection between the pacemaking role of the orbital forcing and the observed irregularity of the glacial terminations during the late Pleistocene, cf. Broecker and Van Donk (1970) and Ghil and Childress (1987, Fig. 11.2).

Based on the considerable success of NDS and RDS applications to other climate problems — such as ENSO (Ghil et al., 2008; Ghil and Zaliapin, 2015; Chekroun et al., 2018; Marangio et al., 2019), the wind-driven ocean circulation (Pierini et al., 2016, 2018) or the evaluation of the ensemble simulations routinely performed in support of the Assessment Reports of the Intergovernmental Panel on Climate Change (Drótos et al., 2015; Vissio et al., 2020) — it would appear worthwhile to proceed further along these lines.

https://doi.org/10.5194/cp-2021-136
Preprint. Discussion started: 14 October 2021

Climate of the Past Discussions
Open Access
EGU

Of course, each of these problems requires one or more distinct climate models, as well as very careful modeling of the kinds of time-dependent changes in forcing and parameters that are most enlightening, as well as most relevant and plausible. A good way would be to start testing ideas with relatively simple models and pursue the investigation systematically across a hierarchy of models — through intermediate ones and on to the most detailed ones — in order to further increase understanding of the climate system and of its predictability on the various paleoclimatic time scales mentioned in the list above.

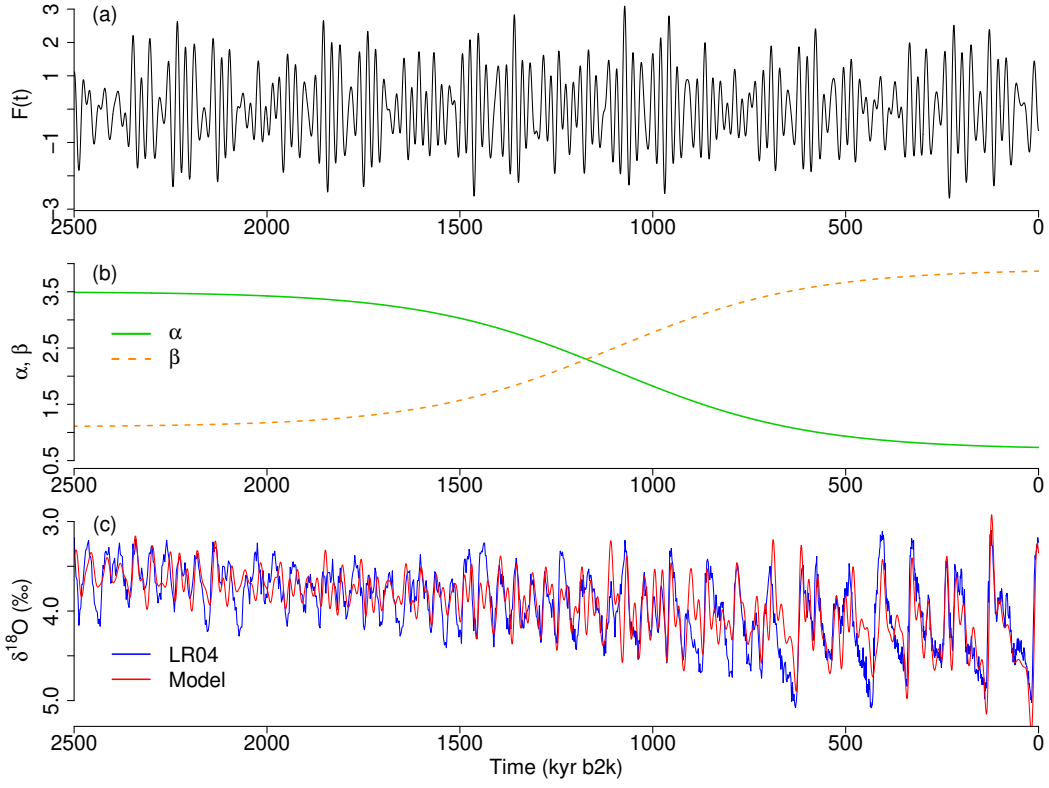

Figure 10. Glacial-interglacial cycles simulated by the modified Daruka and Ditlevsen model of Eqs. (29, 30): (a) June 21 insolation $F(t)$ at 65°N, normalized to have mean zero and unit standard deviation over the last 1 000 kyr. (b) Slowly changing parameters $\alpha(t)$ and $\beta(t)$ introduced to give rise to the MPT. (c) Simulated glacial-interglacial cycles $\delta^{18}\mathrm{O}_{\mathrm{model}}$ (red) in comparison with the benthic $\delta^{18}\mathrm{O}$ (blue).

Such an approach can usefully complement the more common one of merely pushing onwards to higher and higher model resolution in order to achieve ever more detailed simulations of the system's behavior for a limited set of semi-empirical parameter values. Ghil (2001) and Held (2005), among others, have emphasized the need to pursue such a model hierarchy, as originally proposed by Schneider and Dickinson (1974), in order to balance the need to broaden the number of plausible hypotheses vs the need for confronting them with spatio-temporal details derived from observations.

In this section, we illustrate how the PBA concept can help shed more light upon the dynamics of ice age models. For this purpose, we apply the Daruka and Ditlevsen (2016) model of glacial-interglacial cycles with slight modifications. We show

https://doi.org/10.5194/cp-2021-136
Preprint. Discussion started: 14 October 2021


Climate of the Past Discussions
Open Access
EGU

first that this model approximates rather well the glacial cycles inferred from the benthic δ^{18}O proxy reconstruction of Lisiecki and Raymo (2005) and then compute the model's PBA to investigate the dynamical stability of its glacial cycles.

The model's variables are a global temperature anomaly y that is proportional to minus the global ice volume and an effective climatic memory term x that represents the internal degrees of freedom. In the deterministic case, the governing equations are given by

$$\tau\dot{x} = \lambda y, \tag{29a}$$

$$\tau\dot{y} = -\alpha(t) + x - x^3 - \beta(t)F(t)x - \kappa y; \tag{29b}$$

here t is the time in kyr and $F(t)$ is the normalized June 21 insolation at 65°N, based on the calculations of Laskar et al. (2004), as shown in Fig. 10(a). The constant parameter values are chosen as $\kappa = 1$, $\tau = 100$, and $\lambda = 10$.

The equations (29) generalize a first-order ODE system that is equivalent to the Duffing form of the nonlinear-spring equation (7) discussed in Sec. 2.2. The use of such simple forms of first-order systems in paleoclimate models was initiated by Saltzman et al. (1981). We deviate from Daruka and Ditlevsen (2016), though, by introducing a slow change in the parameters $\alpha(t)$ and $\beta(t)$ of Eq. (29b), as follows:

$$\alpha(t) = 2.1 - 1.4\tanh\left((t+1100)/500\right), \tag{30a}$$

$$\beta(t) = 2.5 + 1.4\tanh\left((t+1100)/500\right). \tag{30b}$$

The functions $\alpha(t)$ and $\beta(t)$ so defined are plotted in Fig. 10(b) and they induce, as we shall see forthwith, a model behavior that resembles the MPT. Moreover, to simulate $\delta^{18}\mathrm{O}_{\mathrm{model}}$, we add a slow linear trend to the slow variable y to mimic the overall cooling at time scales of millions of years, thus: $\delta^{18}\mathrm{O}_{\mathrm{model}} = 4.3 - 1.4y + 0.0003t$.

Figure 10(c) shows a time series of simulated glacial-interglacial changes $\delta^{18}\mathrm{O}_{\mathrm{model}}$ (red) in comparison with the benthic δ^{18}O (blue) of Lisiecki and Raymo (2005). The model's initial condition is taken to be $x = -1$ and $y = 0$ at $t = -10\,000$ kyr and, since the insolation forcing in panel (a) is prescribed as a time series with 100-yr sampling, we solved Eq. (29) using Heun's predictor-corrector method (Isaacson and Keller, 2012, Ch. 8) with a step size of 100 yr. The correlation between the model simulation and the proxy record is 0.75 for the time interval from $-2\,600$ kyr to 0 kyr b2k, and 0.72 over the interval from $-1\,000$ kyr to 0 kyr b2k. Varying the parameters slowly across the time interval of interest, as shown in Fig. 10(b), leads to a change in the frequency — from a dominant 41-kyr periodicity prior to the MPT to a dominant 100-kyr periodicity after the MPT — and a substantial increase in the amplitude.

We next approximate the PBA by taking 40 random initial conditions at 10 Myr b2k and integrating the model of Eqs. (29, 30) up to the present time. The PBA in this case is simply a moving fixed point, as plotted in Fig. 11(a), since the model dynamics is predominantly stable in the long time interval prior to the MPT that is situated around 1.2–0.8 Myr b2k. It would appear, therewith, that the orbital forcing simply moves this fixed point around and fully determines Earth's climate.

However, when keeping the parameters α and β fixed at their post-MPT values $\alpha = 0.7$ and $\beta = 3.9$ throughout the simulation interval and repeating the computation of the PBA, a more complex picture arises. In the latter case, Fig. 11(b) shows a bunching of trajectories into separate clusters, subject to the quasi-periodic orbital forcing of Fig. 10(a).

https://doi.org/10.5194/cp-2021-136
Preprint. Discussion started: 14 October 2021

Climate of the Past Discussions
Open Access
EGU

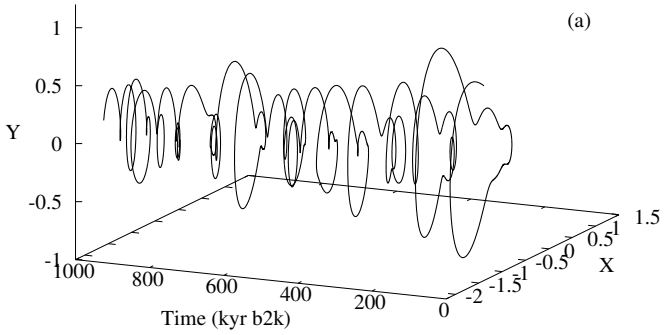

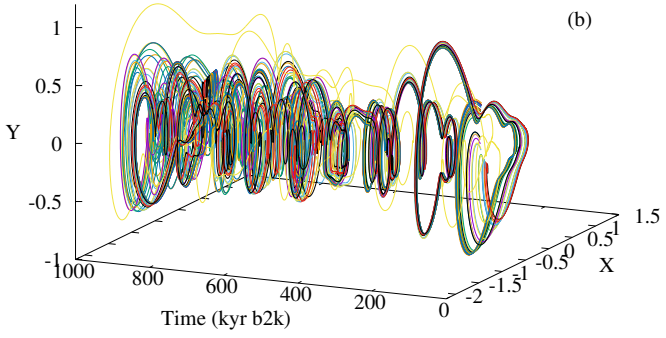

Figure 11. PBA of the modified Daruka and Ditlevsen (2016) model given by Eqs. (29), approximated by forty trajectories starting from random initial conditions in $(x, y) \in [-2, 2] \times [-2, 2]$ at $t = -10\,000$ kyr. (a) The behavior corresponding to Fig. 10, with the slowly changing parameters $\alpha(t)$ and $\beta(t)$ given by Eqs. (30); and (b) the behavior for $\alpha(t)$ and $\beta(t)$ kept constant at the post-MPT values of $\alpha = 0.7$ and $\beta = 3.9$.

There are two interesting inferences to be drawn. First, post-MPT dynamics is much more irregular and unstable than the stable, quasi-periodic dynamics prior to the MPT. This result is consistent with Mitsui et al. (2015), who showed the robustness of the 40-kyr glacial cycles and instability of 100-kyr glacial cycles against perturbations in terms of mode-locking theory and strange nonchaotic attractors. It also appears to be consistent with the Willeit et al. (2019) simulation of the last 3 Myr that used an Earth System Model of Intermediate Complexity (CLIMBER-2) that included ice sheets and a carbon cycle, along

https://doi.org/10.5194/cp-2021-136
Preprint. Discussion started: 14 October 2021


Climate of the Past Discussions

with atmosphere-ocean variables. In their work, trajectories starting from different initial states tended to converge to a single attracting trajectory in the Early Pleistocene, while several distinct trajectories survived in the Late Pleistocene after the MPT.

Second, the separate bundles or "ropes" of trajectories in Fig. 11(b) seem to point to the type of *generalized synchronization* discussed in the paleoclimate context by De Saedeleer et al. (2013) and in the context of interannual and interdecadal climate variability by Pierini and Ghil (2021) and Vannitsem et al. (2021). Generalized synchronization in the strict sense of the existence of a map between a time-dependent control and the system's asymptotic behavior has only been shown to hold for nonchaotic systems. Work is under way, though, to further generalize this concept to chaotic systems as well (e.g., Rulkov et al., 1995; Zhang et al., 2007).

5 Conclusions

In this review-and-research paper, we have covered in Sec. 1 the contributions of the 1970s to the rebirth of the Milankovitch (1920) theory of the ice ages and in Sec. 2 the 1980s advances in modeling the Quaternary climate's intrinsic variability. In Sec. 3, we presented first results on the interaction between the orbital insolation forcing of Sec. 1 and the intrinsic variability of Sec. 2, and proceeded to introduce the novel concepts and tools of the theory of nonautonomous and random dynamical systems (NDSs and RDSs) that can help to better model and understand this interaction. The section concluded by the formulation and study of a FitzHugh-Nagumo (FHN)-type model of recurrent Dansgaard-Oeschger (D-O) events, in which historical CO_2 concentrations induced episodes of D-O events alternating with episodes of their absence, in excellent qualitative agreement with NGRIP δ^{18}O data; see again Fig. 9.

Finally, in Sec. 4, we listed a number of open issues on Quaternary and longer paleoclimate time scales, and proposed to address them by using the tools of Sec. 3.2. This approach was illustrated by a Duffing-type model of Daruka and Ditlevsen (2016), modified to include slow changes in the parameters that mimic such changes in the Earth system over the duration of the Quaternary period.

When the parameters are gradually changed in time so as to exhibit the mid-Pleistocene transition (MPT), the PBA is simply a moving fixed point. However, when the parameters are fixed at their post-MPT values, the PBA so obtained is chaotic and exhibits clusters of trajectories that we termed *ropes*. This suggests (a) that the stability of the system is gradually lost while crossing the MPT; and (b) that Late Pleistocene climate, albeit chaotic, may well be subject to a kind of generalized synchronization (cf. De Saedeleer et al., 2013; Pierini and Ghil, 2021; Vannitsem et al., 2021) with the orbital forcing that is illustrated in Fig. 4 of Sec. 3.1 herein. In the specific situation at hand, separate ropes may be associated with various combination tones of the forcing frequencies.

In a broader perspective — and leaving aside various finer points of the MPT conversation outlined in Sec. 2.2 — one can see the work that was reviewed and extended in this paper as a confirmation of the fine intuition of Emiliani and Geiss (1959), six decades ago, as summarized in and further expanded by Ghil and Childress (1987, Sec. 12, pp. 446-447):

"Hence the following scenario (compare Emiliani and Geiss, 1959) suggests itself for the successive climatic transitions from Pliocene to Pleistocene and from Early to Late Pleistocene: As land masses moved towards more northerly positions, small

https://doi.org/10.5194/cp-2021-136
Preprint. Discussion started: 14 October 2021


Climate of the Past Discussions

ice caps formed on mountain chains and at high latitudes. These ice caps, due to their feedback on albedo, made climate more sensitive to insolation variations than it was in the total absence of ice. The response of the climatic system to such variations during the Early Pleistocene (2 000 [kyr]–1 000 [kyr] ago) was still relatively weak, of a fraction of a degree centigrade in global temperature perhaps, in agreement with the quasi-equilibrium results of Section 10.2.

As ice caps passed, about 1 000 [kyr] ago, a certain critical size, the unforced system jumped from its stable equilibrium to its stable limit-cycle state (Figures 12.5 and 12.9), increasing dramatically the climate's total variability, to a few degrees centigrade in global temperature. Furthermore, resonant response became possible (see also Oerlemans (1984) [in Berger et al. (1984)] and Sergin (1979)), enhancing abruptly the amplitude of the peak at 100 [kyr], among others."

The take-home message is that slow and fast processes, both intrinsic and extrinsic, interact on all paleoclimatic time scales and that we are mastering the art of modeling such interactions.

Code and data availability. All code used to generate the figures presented in this article is available from the authors upon request. NGRIP δ^{18}O and the historical CO_2 data shown in Fig. 9 are available from https://www.iceandclimate.nbi.ku.dk/data/ (last accessed: 2. September 2021) and as a supplement to Seierstad et al. (2014), respectively. The benthic δ^{18}O data shown in Fig. 10 have been obtained from https://lorraine-lisiecki.com/LR04stack.txt (last accessed: 2. September 2021).

Video supplement. The video supplement to this article illustrates the pullback attractor (PBA) associated with the simple system governed by Eqs. (16) and (17). It shows a heat map of the phase plane, derived from an increasing number of trajectories with common initial time $t_\mathrm{i} = -200$ and final time $t_\mathrm{f} = 200$. The initial radius and phase of each trajectory are randomly sampled from Gaussian distributions centered at $\mu_\rho = 20$ and $\mu_\phi = 0$ with standard deviations of $\sigma_\rho = 5$ and $\sigma_\phi = 10$, respectively. Over the course of the video, 100 trajectories are continuously added to the heat map and the annular disc $\mathcal{D} = \{(\rho,\phi) : \rho \in [\mu - \alpha\beta, \mu + \alpha\beta] \text{ and } \phi \in [0, 2\pi)\}$ fills up. The heat map in Fig. 5(b) is a snapshot from this video at time $t = 0.2$.

Appendix A: PBA for a limit cycle with sinusoidally modulated radius

Here we study the system of two formally decoupled ODEs

$$\frac{d\rho}{dt} = \alpha(\mu + \beta\sin(\nu t) - \rho), \quad \frac{d\phi}{dt} = \omega \qquad \text{with} \qquad \rho > 0,\ \mu > 0 \tag{A1}$$

that was introduced in Sec. 3.2 and analytically derive its invariant sets

$$\mathcal{A}(t) = \{\big(\alpha\beta\sin(\nu t + \vartheta) + \mu, \varphi\big) : \varphi \in [0, 2\pi)\} \qquad \forall t \in \mathbb{R}, \tag{A2}$$

as well as the corresponding pullback attractor (PBA). Following Crauel and Kloeden (2015), the PBA is given by the family

$$\mathscr{A} = \{\mathcal{A}\}_{t:t\in\mathbb{R}} \tag{A3}$$

https://doi.org/10.5194/cp-2021-136
Preprint. Discussion started: 14 October 2021

Climate of the Past Discussions
Open Access
EGU

First, we define $\Delta\rho(t) = \rho(t) - \mu$, which gives rise to

$$\frac{\mathrm{d}\Delta\rho(t)}{\mathrm{d}t} = -\alpha\Delta\rho(t) + \alpha\beta\sin(\nu t). \tag{A4}$$

This is an inhomogeneous ODE and can thus be solved by the variation of parameters method (e.g., Boyce and DiPrima, 2005).

The Ansatz

$$\Delta\rho(t) = c(t)\, e^{-\alpha(t-t_0)} \tag{A5}$$

yields

$$\frac{\mathrm{d}\Delta\rho(t)}{\mathrm{d}t} = -\alpha\Delta\rho(t) + \frac{\mathrm{d}c(t)}{\mathrm{d}t}\, e^{-\alpha(t-t_0)}. \tag{A6}$$

A comparison with Eq. (A4) requires

$$\frac{\mathrm{d}}{\mathrm{d}t}c(t) = \alpha\beta\sin(\nu t)e^{+\alpha(t-t_0)}, \tag{A7}$$

and hence

$$c(t) = \int_{t_0}^{t} \alpha\beta\sin(\nu t')e^{+\alpha(t'-t_0)}\mathrm{d}t' + \gamma = [\alpha\beta\sin(\nu t')\frac{1}{\alpha}e^{+\alpha(t'-t_0)}]_{t_0}^{t} - \int_{t_0}^{t}\frac{\nu}{\alpha}\alpha\beta\cos(\nu t')e^{+\alpha(t'-t_0)}\mathrm{d}t' + \gamma. \tag{A8}$$

Repeated partial integration yields

$$\int_{t_0}^{t}\frac{\nu}{\alpha}\alpha\beta\cos(\nu t')e^{+\alpha(t'-t_0)}\mathrm{d}t' = [\frac{\nu}{\alpha}\alpha\beta\cos(\nu t')\frac{1}{\alpha}e^{+\alpha(t'-t_0)}]_{t_0}^{t} + \int_{t_0}^{t}\frac{\nu^2}{\alpha^2}\alpha\beta\sin(\nu t')e^{+\alpha(t'-t_0)}\mathrm{d}t'. \tag{A9}$$

Therefore, we find

$$(1+\frac{\nu^2}{\alpha^2})\int_{t_0}^{t}\alpha\beta\sin(\nu t')e^{+\alpha(t'-t_0)}\mathrm{d}t' = [\alpha\beta\sin(\nu t')\frac{1}{\alpha}e^{+\alpha(t'-t_0)}]_{t_0}^{t} - [\frac{\nu}{\alpha}\alpha\beta\cos(\nu t')\frac{1}{\alpha}e^{+\alpha(t'-t_0)}]_{t_0}^{t} \tag{A10}$$

and finally

$$c(t) = \frac{1}{(1+\frac{\nu^2}{\alpha^2})}\left(\underbrace{[\beta\sin(\nu t')e^{+\alpha(t'-t_0)}]_{t_0}^{t}}_{=\beta[\sin(\nu t)e^{\alpha(t-t_0)}-\sin(\nu t_0)]} - \underbrace{[\frac{\nu\beta}{\alpha}\cos(\nu t')e^{+\alpha(t'-t_0)}]_{t_0}^{t}}_{=\frac{\nu\beta}{\alpha}[\cos(\nu t)e^{\alpha(t-t_0)}-\cos(\nu t_0)]} + \gamma\right). \tag{A11}$$

Plugging this result into the Ansatz (A5) yields

$$\Delta\rho(t,t_0) = \frac{1}{(1+\frac{\nu^2}{\alpha^2})}\left(\beta[\sin(\nu t) - \sin(\nu t_0)e^{-\alpha(t-t_0)}] - \frac{\nu\beta}{\alpha}[\cos(\nu t) - \cos(\nu t_0)e^{-\alpha(t-t_0)}]\right) + \gamma e^{-\alpha(t-t_0)}, \tag{A12}$$

with the initial conditions

$$\Delta\rho(t_0,t_0) = \gamma. \tag{A13}$$

https://doi.org/10.5194/cp-2021-136
Preprint. Discussion started: 14 October 2021

Climate of the Past Discussions

In the pullback limit, all the terms that carry a factor $e^{-\alpha(t-t_0)}$ vanish and thus

$$\lim_{t_0\to-\infty}\Delta\rho(t,t_0)=\frac{1}{(1+\frac{\nu^2}{\alpha^2})}\left(\beta\sin(\nu t)-\frac{\nu\beta}{\alpha}\cos(\nu t)\right)=\alpha\beta\sin(\nu t+\vartheta), \tag{A14}$$

with $\vartheta=\arctan(-\nu/\alpha)$. For comparison, the modulation of the target radius itself was given by $\beta\sin(\nu t)$ and hence it is amplified by the factor of α. Since ρ is restricted to positive values, this solution requires $\alpha\beta<\mu$.

Since the evolution in time of the phase $\phi(t)$ is trivial, different initial conditions for the phase do not converge. Hence, the time-dependent sets that are invariant with respect to the dynamics of the system are

$$\mathcal{A}(t)=\{(\rho(t),\phi):\phi\in[0,2\pi)\}=\{(\alpha\beta\sin(\nu t+\vartheta),\phi):\phi\in[0,2\pi)\}. \tag{A15}$$

Defined as the indexed family of all $\mathcal{A}(t)$, the system's PBA is comprised of the family of circles

$$\mathscr{A}=\{A(t)\}_{t\in\mathbb{R}}=\{(\alpha\beta\sin(\nu t+\vartheta),\phi):\phi\in[0,2\pi)\}_{t\in\mathbb{R}}. \tag{A16}$$

Author contributions. MG conceived and designed the study. KR and TM carried out the numerical computations. All authors interpreted and discussed the results and wrote the manuscript.

Competing interests. The authors declare that they have no conflict of interest.

Acknowledgements. We thank Andreas Groth for helpful comments on an earlier version of this manuscript. TM and NB acknowledge funding by the Volkswagen Foundation. The present work is TiPES contribution #52; the TiPES (Tipping Points in the Earth System) project has received funding from the European Union's Horizon 2020 research and innovation program under Grant Agreement No. 820970. MG acknowledges support by the EIT Climate-KIC; EIT Climate-KIC is supported by the European Institute of Innovation & Technology (EIT), a body of the European Union.

https://doi.org/10.5194/cp-2021-136
Preprint. Discussion started: 14 October 2021

References

Arnol'd, V. I.: Geometrical Methods in the Theory of Ordinary Differential Equations, Springer Science & Business Media; first Russian edition 1978, 2012.

Ashwin, P. and Ditlevsen, P.: The middle Pleistocene transition as a generic bifurcation on a slow manifold, Climate Dynamics, 45, 2683–2695, 2015.

Bagniewski, W., Ghil, M., and Rousseau, D.-D.: Abrupt transition detection in paleorecords: A new methodology, submitted, 2021.

Bereiter, B., Eggleston, S., Schmitt, J., Nehrbass-Ahles, C., Stocker, T. F., Fischer, H., Kipfstuhl, S., and Chappellaz, J.: Revision of the EPICA Dome C CO2 record from 800 to 600 kyr before present, Geophysical Research Letters, 42, 542–549, 2015.

Berger, A.: Long-term variations of daily insolation and Quaternary climatic changes, Journal of the Atmospheric Sciences, 35, 2362–2367, 1978.

Berger, A., Imbrie, J., Hays, J., Kukla, G., and Saltzman, B., eds.: Milankovitch and Climate: Understanding the Response to Astronomical Forcing, vols. I & II, D. Reidel Publ. Co., Dordrecht/Boston, reissued in 2013 by Springer Science & Business Media, 1984.

Bódai, T. and Tél, T.: Annual variability in a conceptual climate model: Snapshot attractors, hysteresis in extreme events, and climate sensitivity, Chaos: An Interdisciplinary Journal of Nonlinear Science, 22, 023110, https://doi.org/http://dx.doi.org/10.1063/1.3697984, 2012.

Bódai, T., Lucarini, V., Lunkeit, F., and Boschi, R.: Global instability in the Ghil-Sellers model, Climate Dynamics, 44, 3361–3381, 2015.

Boers, N., Chekroun, M. D., Liu, H., Kondrashov, D., Rousseau, D.-D., Svensson, A., Bigler, M., and Ghil, M.: Inverse stochastic–dynamic models for high-resolution Greenland ice core records, Earth System Dynamics, 8, 1171–1190, https://doi.org/10.5194/esd-8-1171-2017, 2017a.

Boers, N., Goswami, B., and Ghil, M.: A complete representation of uncertainties in layer-counted paleoclimatic archives, Climate of the Past, 13, 1169–1180, https://doi.org/10.5194/cp-13-1169-2017, 2017b.

Boers, N., Ghil, M., and Rousseau, D.-D.: Ocean circulation, ice shelf, and sea ice interactions explain Dansgaard–Oeschger cycles, Proceedings of the National Academy of Sciences, 115, E11 005–E11 014, https://doi.org/10.1073/pnas.1802573115, 2018.

Bond, G., Showers, W., Cheseby, M., Peter Almasi, R. L., deMenocal, P., Priore, P., Irka Hajdas, H. C., and Bonani, G.: A pervasive millennial-scale cycle in North Atlantic Holocene and glacial climates, Science, 278, 1257–1266, https://doi.org/10.1126/science.278.5341.1257, 1997.

Boyce, W. E. and DiPrima, R. C.: Elementary Differential Equations and Boundary Value Problems, 8th Edition, John Wiley & Sons, 2005.

Broecker, W. S. and Van Donk, J.: Insolation changes, ice volumes, and the O^{18} record in deep-sea cores, Reviews of Geophysics, 8, 169–198, 1970.

Budyko, M. I.: The effect of solar radiation variations on the climate of the Earth, Tellus, 21, 611–619, 1969.

Caraballo, T. and Han, X.: Applied Nonautonomous and Random Dynamical Systems: Applied Dynamical Systems, Springer Science + Business Media, 2017.

Charó, G. D., Chekroun, M. D., Sciamarella, D., and Ghil, M.: Noise-driven topological changes in chaotic dynamics, arXiv:2010.09611v7 [nlin.CD], 2021.

Chekroun, M. D., Simonnet, E., and Ghil, M.: Stochastic climate dynamics: random attractors and time-dependent invariant measures, Physica D: Nonlinear Phenomena, 240, 1685–1700, https://doi.org/10.1016/j.physd.2011.06.005, 2011.

https://doi.org/10.5194/cp-2021-136
Preprint. Discussion started: 14 October 2021

Chekroun, M. D., Ghil, M., and Neelin, J. D.: Pullback attractor crisis in a delay differential ENSO model, in: Advances in Nonlinear Geosciences, edited by Tsonis, A. A., pp. 1–33, Springer Science & Business Media, https://doi.org/10.1007/978-3-319-58895-7, 2018.

Crafoord, C. and Källén, E.: A note on the condition for existence of more than one steady state solution in Budyko-Sellers type models, J. Atmos. Sci, 35, 1123–1125, 1978.

Crauel, H. and Kloeden, P. E.: Nonautonomous and random attractors, Jahresbericht der Deutschen Mathematiker-Vereinigung, 117, 173–206, 2015.

Crucifix, M.: Oscillators and relaxation phenomena in Pleistocene climate theory, Philosophical Transactions of the Royal Society A: Mathematical, Physical and Engineering Sciences, 370, 1140–1165, 2012.

Crucifix, M.: Why could ice ages be unpredictable?, Clim. Past, 9, 2253–2267, 2013.

Dansgaard, W., Johnsen, S. J., Clausen, H. B., Dahl-Jensen, D., Gundestrup, N. S., Hammer, C. U., Hvidberg, C. S., Steffensen, J. P., Sveinbjörnsdottir, A. E., Jouzel, J., and Bond, G.: Evidence for general instability of past climate from a 250-kyr ice-core record, Nature, 364, 218–220, https://doi.org/10.1038/364218a0, 1993.

Daruka, I. and Ditlevsen, P. D.: A conceptual model for glacial cycles and the middle Pleistocene transition, Climate Dynamics, 46, 29–40, 2016.

De Saedeleer, B., Crucifix, M., and Wieczorek, S.: Is the astronomical forcing a reliable and unique pacemaker for climate? a conceptual model study, Climate Dynamics, 40, 273–294, 2013.

Ditlevsen, P., Mitsui, T., and Crucifix, M.: Crossover and peaks in the Pleistocene climate spectrum; understanding from simple ice age models, Climate Dynamics, 54, 1801–1818, 2020.

Ditlevsen, P. D. and Ashwin, P. B.: Complex climate response to astronomical forcing: The middle-Pleistocene transition in glacial cycles and changes in frequency locking, Frontiers in Physics, 6, https://doi.org/10.3389/fphy.2018.00062, 2018.

Ditlevsen, P. D., Andersen, K. K., and Svensson, A.: The DO-climate events are probably noise induced: Statistical investigation of the claimed 1470 years cycle, Climate of the Past, 3, 129–134, https://doi.org/10.5194/cp-3-129-2007, 2007.

Drótos, G., Bódai, T., and Tél, T.: Probabilistic concepts in a changing climate: A snapshot attractor picture, Journal of Climate, 28, 3275–3288, 2015.

Duffing, G.: Erzwungene Schwingungen bei veränderlicher Eigenfrequenz und ihre technische Bedeutung, vol. 41/42 of *Sammlung Vieweg*, R. Vieweg & Sohn, Braunschweig, 1918.

Einstein, A.: Über die von der molekularkinetischen Theorie der Wärme geforderte Bewegung von in ruhenden Flüssigkeiten suspendierten Teilchen, Annalen der Physik, 322, 549–560; reprinted in *Investigations on the Theory of the Brownian Movement, five articles by A. Einstein*, R. Furth (ed.) and A. D. Cowper (transl.), 1956, Dover Publ., New York, 122 pp., 1905.

Emiliani, C. and Geiss, J.: On glaciations and their causes, Geologische Rundschau, 46, 576–601, 1959.

Fienga, A., Laskar, J., Exertier, P., Manche, H., and Gastineau, M.: Numerical estimation of the sensitivity of INPOP planetary ephemerides to general relativity parameters, Celestial Mechanics and Dynamical Astronomy, 123, 325–349, 2015.

FitzHugh, R.: Impulses and physiological states in theoretical models of nerve membrane, Biophysical journal, 1, 445–466, 1961.

Flint, R. F.: Glacial and Quaternary Geology, Wiley New York, 1971.

Ghil, M.: Climate stability for a Sellers-type model, Journal of the Atmospheric Sciences, 33, 3–20, 1976.

Ghil, M.: Climate sensitivity, energy balance models, and oscillatory climate models, Journal of Geophysical Research: Atmospheres, 89, 1280–1284, 1984.

Ghil, M.: Cryothermodynamics: the chaotic dynamics of paleoclimate, Physica D, 77, 130–159, 1994.

https://doi.org/10.5194/cp-2021-136
Preprint. Discussion started: 14 October 2021

Ghil, M.: Hilbert problems for the geosciences in the 21st century, Nonlinear Processes in Geophysics, 8, 211–211, https://doi.org/10.5194/npg-8-211-2001, 2001.

Ghil, M.: Climate variability: Nonlinear and random aspects, in: Encyclopedia of Atmospheric Sciences, 2nd edn., edited by G. R. North, J. P. and Zhang, F., vol. 2, pp. 38–46, Elsevier, 2014.

Ghil, M.: A century of nonlinearity in the geosciences, Earth and Space Science, 6, 1007–1042, https://doi.org/10.1029/2019EA000599, 2019.

Ghil, M. and Childress, S.: Topics in Geophysical Fluid Dynamics: Atmospheric Dynamics, Dynamo Theory, and Climate Dynamics, Springer Science+Business Media, Berlin/Heidelberg, https://doi.org/10.1007/978-1-4612-1052-8, Reissued in pdf, 2012, 1987.

Ghil, M. and Le Treut, H.: A climate model with cryodynamics and geodynamics, Journal of Geophysical Research: Oceans, 86, 5262–5270, 1981.

Ghil, M. and Lucarini, V.: The physics of climate variability and climate change, Reviews of Modern Physics, 92, 035 002, https://doi.org/10.1103/RevModPhys.92.035002, 2020.

Ghil, M. and Tavantzis, J.: Global Hopf bifurcation in a simple climate model, SIAM Journal on Applied Mathematics, 43, 1019–1041, https://doi.org/10.1137/0143067, 1983.

Ghil, M. and Vautard, R.: Interdecadal oscillations and the warming trend in global temperature time series, Nature, 350, 324–327, 1991.

Ghil, M. and Zaliapin, I.: Understanding ENSO variability and its extrema: A delay differential equation approach, in: Extreme Events: Observations, Modeling and Economics, Geophysical Monograph 214, edited by Chavez, M., Ghil, M., and Urrutia-Fucugauchi, J., pp. 63–78, Wiley Online Library, 2015.

Ghil, M., Mullhaupt, A., and Pestiaux, P.: Deep water formation and Quaternary glaciations, Climate Dynamics, 2, 1–10, 1987.

Ghil, M., Chekroun, M. D., and Simonnet, E.: Climate dynamics and fluid mechanics: natural variability and related uncertainties, Physica D: Nonlinear Phenomena, 237, 2111–2126, https://doi.org/10.1016/j.physd.2008.03.036, 2008.

Guckenheimer, J. and Holmes, P. J.: Nonlinear Oscillations, Dynamical Systems, and Bifurcations of Vector Fields, Applied Mathematical Sciences, Springer Science & Business Media, 1983.

Hasselmann, K.: Stochastic climate models. I: Theory, Tellus, 28, 473–485, 1976.

Hays, J. D., Imbrie, J., Shackleton, N. J., et al.: Variations in the Earth's orbit: pacemaker of the ice ages, science, 194, 1121–1132, 1976.

Heinrich, H.: Origin and consequences of cyclic ice rafting in the Northeast Atlantic Ocean during the past 130,000 years, Quaternary Research, 29, 142–152, https://doi.org/10.1016/0033-5894(88)90057-9, 1988.

Held, I. M.: The gap between simulation and understanding in climate modeling, Bulletin of the American Meteorological Society, 86, 1609–1614, https://doi.org/10.1175/bams-86-11-1609, 2005.

Held, I. M. and Suarez, M. J.: Simple albedo feedback models of the ice caps, Tellus, 26, 613–629, 1974.

Henry, L. G., McManus, J. F., Curry, W. B., Roberts, N. L., Piotrowski, A. M., and Keigwin, L. D.: North Atlantic ocean circulation and abrupt climate change during the last glaciation, Science, 353, 470–474, https://doi.org/10.1126/science.aaf5529, 2016.

Hoffman, P. F., Kaufman, A. J., Halverson, G. P., and Schrag, D. P.: A Neoproterozoic snowball earth, Science, 281, 1342–1346, 1998.

Huybers, P. J.: Pleistocene glacial variability as a chaotic response to obliquity forcing, Climate of the Past, 2009.

Imbrie, J. and Imbrie, K. P.: Ice Ages: Solving the Mystery, 2nd ed., Harvard University Press, 1986.

Isaacson, E. and Keller, H. B.: Analysis of numerical methods, Dover Publications, Inc., New York, NY, 2012.

Jackson, E. A.: Perspectives of Nonlinear Dynamics, Cambridge University Press, New York, 1991.

https://doi.org/10.5194/cp-2021-136
Preprint. Discussion started: 14 October 2021

Jordan, D. W. and Smith, P.: Nonlinear Ordinary Differential Equations – An Introduction for Scientists and Engineers, Oxford University Press, Oxford/New York, 2 edn., 1987.

Källén, E., Crafoord, C., and Ghil, M.: Free oscillations in a climate model with ice-sheet dynamics, Journal of the Atmospheric Sciences, 36, 2292–2303, 1979.

Kwasniok, F.: Analysis and modelling of glacial climate transitions using simple dynamical systems, Philosophical Transactions of the Royal Society A: Mathematical, Physical and Engineering Sciences, 371, https://doi.org/10.1098/rsta.2011.0472, 2013.

Landau, L. D. and Lifshitz, E. M.: Mechanics, vol. I of Course on Theoretical Physics, Pergamon Press, Oxford, 1960.

Laskar, J., Robutel, P., Joutel, F., Gastineau, M., Correia, A., and Levrard, B.: A long-term numerical solution for the insolation quantities of the Earth, Astronomy & Astrophysics, 428, 261–285, 2004.

Le Treut, H. and Ghil, M.: Orbital forcing, climatic interactions, and glaciation cycles, Journal of Geophysical Research: Oceans, 88, 5167–5190, 1983.

Le Treut, H., Portes, J., Jouzel, J., and Ghil, M.: Isotopic modeling of climatic oscillations: Implications for a comparative study of marine and ice core records, Journal of Geophysical Research: Atmospheres, 93, 9365–9383, 1988.

Lenssen, N. J. L., Schmidt, G. A., Hansen, J. E., Menne, M. J., Persin, A., Ruedy, R., and Zyss, D.: Improvements in the GISTEMP uncertainty model, Journal of Geophysical Research: Atmospheres, 124, 6307–6326, 2019.

Lisiecki, L. E. and Raymo, M. E.: A Pliocene-Pleistocene stack of 57 globally distributed benthic δ18O records, Paleoceanography, 20, 2005.

Lorenz, E. N.: Deterministic nonperiodic flow, Journal of the Atmospheric Sciences, 20, 130–141, 1963.

Marangio, L., Sedro, J., Galatolo, S., Di Garbo, A., and Ghil, M.: Arnold maps with noise: Differentiability and non-monotonicity of the rotation number, Journal of Statistical Physics, 179, 1–31, https://doi.org/10.1007/s10955-019-02421-1, 2019.

Milankovitch, M.: Théorie mathématique des phénomènes thermiques produits par la radiation solaire, Gauthier-Villars, Paris, 1920.

Mitsui, T. and Crucifix, M.: Influence of external forcings on abrupt millennial-scale climate changes: a statistical modelling study, Climate Dynamics, 48, 2729–2749, 2017.

Mitsui, T., Crucifix, M., and Aihara, K.: Bifurcations and strange nonchaotic attractors in a phase oscillator model of glacial–interglacial cycles, Physica D: Nonlinear Phenomena, 306, 25–33, 2015.

Nagumo, J., Arimoto, S., and Yoshizawa, S.: An active pulse transmission line simulating nerve axon, Proceedings of the IRE, 50, 2061–2070, 1962.

National Research Council: Understanding Climatic Change, a Program for Action, National Academy of Sciences, Washington, DC, 239 pages, 1975.

North, G. R.: Analytical solution to a simple climate model with diffusive heat transport, Journal of the Atmospheric Sciences, 32, 1301–1307, 1975.

North Greenland Ice Core Project members: High-resolution record of the Northern Hemisphere climate extending into the last interglacial period, Nature, 431, 147–151, 2004.

Oerlemans, J.: On the origin of the ice ages, in: Milankovitch and Climate: Understanding the Response to Astronomical Forcing, vols. I & II, edited by Berger, A., Imbrie, J., Hays, J., Kukla, G., and Saltzman, B., pp. 607–611, D. Reidel Publ. Co., 1984.

Pierini, S. and Ghil, M.: Climate tipping points induced by parameter drift: an excitable system study, Scientific Reports, in press, 2021.

Pierini, S., Ghil, M., and Chekroun, M. D.: Exploring the pullback attractors of a low-order quasigeostrophic ocean model: The deterministic case, Journal of Climate, 29, 4185–4202, 2016.

https://doi.org/10.5194/cp-2021-136
Preprint. Discussion started: 14 October 2021

Pierini, S., Chekroun, M. D., and Ghil, M.: The onset of chaos in nonautonomous dissipative dynamical systems: A low-order ocean–model case study, Nonlin. Processes Geophys., 25, 671–692, https://doi.org/10.5194/npg-25-671-2018, 2018.

Pierrehumbert, R. T.: High levels of atmospheric carbon dioxide necessary for the termination of global glaciation, Nature, 429, 646–649, https://doi.org/10.1038/nature02640, 2004.

Rasmussen, S. O., Bigler, M., Blockley, S. P., Blunier, T., Buchardt, S. L., Clausen, H. B., Cvijanovic, I., Dahl-Jensen, D., Johnsen, S. J., Fischer, H., et al.: A stratigraphic framework for abrupt climatic changes during the Last Glacial period based on three synchronized Greenland ice-core records: refining and extending the INTIMATE event stratigraphy, Quaternary Science Reviews, 106, 14–28, 2014.

Rial, J. A. and Yang, M.: Is the frequency of abrupt climate change modulated by the orbital insolation?, Geophysical Monograph Series, 173, 167–174, https://doi.org/10.1029/173GM12, 2007.

Rousseau, D.-D., Bagniewski, W., and Ghil, M.: Abrupt climate changes and the astronomical theory, Climate of the Past, in this issue, https://doi.org/10.5194/cp-2021-103, 2021.

Ruddiman, W. F. and McIntyre, A.: The North Atlantic Ocean during the last deglaciation, Palaeogeography, Palaeoclimatology, Palaeoecology, 35, 145–214, 1981.

Rulkov, N. F., Sushchik, M. M., Tsimring, L. S., and Abarbanel, H. D. I.: Generalized synchronization of chaos in directionally coupled chaotic systems, Physical Review E, 51, 980–994, https://doi.org/10.1103/physreve.51.980, 1995.

Saltzman, B. and Maasch, K. A.: Carbon cycle instability as a cause of the late Pleistocene ice age oscillations: modeling the asymmetric response, Global Biogeochemical Cycles, 2, 177–185, 1988.

Saltzman, B. and Sutera, A.: The mid-Quaternary climatic transition as the free response of a three-variable dynamical model, Journal of the Atmospheric Sciences, 44, 236–241, 1987.

Saltzman, B., Sutera, A., and Evenson, A.: Structural stochastic stability of a simple auto-oscillatory climatic feedback system, Journal of the Atmospheric Sciences, 38, 494–503, 1981.

Schneider, S. H. and Dickinson, R. E.: Climate modelling, Reviews of Geophysics and Space Physics, 25, 447–493, 1974.

Seierstad, I. K., Abbott, P. M., Bigler, M., Blunier, T., Bourne, A. J., Brook, E., Buchardt, S. L., Buizert, C., Clausen, H. B., Cook, E., Dahl-Jensen, D., Davies, S. M., Guillevic, M., Johnsen, S. J., Pedersen, D. S., Popp, T. J., Rasmussen, S. O., Severinghaus, J. P., Svensson, A., and Vinther, B. M.: Consistently dated records from the Greenland GRIP, GISP2 and NGRIP ice cores for the past 104 ka reveal regional millennial-scale δ18O gradients with possible Heinrich event imprint, Quaternary Science Reviews, 106, 29–46, https://doi.org/https://doi.org/10.1016/j.quascirev.2014.10.032, https://www.sciencedirect.com/science/article/pii/S027737911400434X, dating, Synthesis, and Interpretation of Palaeoclimatic Records and Model-data Integration: Advances of the INTIMATE project(INTegration of Ice core, Marine and TErrestrial records, COST Action ES0907), 2014.

Sellers, W. D.: A global climatic model based on the energy balance of the Earth atmosphere, Journal of Applied Meteorology, 8, 392–400, 1969.

Sergin, V. Y.: Numerical modeling of the glaciers-ocean-atmosphere global system, Journal of Geophysical Research: Oceans, 84, 3191–3204, 1979.

SMIC: Inadvertent Climate Modification: Report of the Study of Man's Impact on Climate, The MIT Press, Cambridge, Mass., 308 pp., 1971.

Tziperman, E. and Gildor, H.: The stabilization of the thermohaline circulation by the temperature–precipitation feedback, Journal of Physical Oceanography, 32, 2707–2714, 2002.

Van der Pol, B.: On relaxation-oscillations, The London, Edinburgh and Dublin Phil. Mag. and J. Sci., 2, 978–992, 1926.

https://doi.org/10.5194/cp-2021-136
Preprint. Discussion started: 14 October 2021

Vannitsem, S., Demaeyer, J., and Ghil, M.: Extratropical low-frequency variability with ENSO forcing: A reduced-order coupled model study, J. Adv. Model. Earth Syst., p. e2021MS002530, 2021.

Varadi, F., Runnegar, B., and Ghil, M.: Successive refinements in long-term integrations of planetary orbits, The Astrophysical Journal, 592, 620–630, 2003.

Vettoretti, G., Ditlevsen, P., Jochum, M., and Rasmussen, S. O.: Millennial-scale Ice Age Climate Oscillations Controlled by Atmospheric CO2, Nature Geoscience, under review.

Vissio, G., Lembo, V., Lucarini, V., and Ghil, M.: Evaluating the performance of climate models based on Wasserstein distance, Geophysical Research Letters, 47, e2020GL089 385, https://doi.org/10.1029/2020GL089385, 2020.

Weertman, J.: Rate of growth or shrinkage of non-equilibrium ice-sheets, J. Glaciology, 6, 145–158, 1964.

Weertman, J.: Milankovitch solar radiation variations and ice-age ice-sheet sizes, Nature, 261, 17–20, 1976.

Westerhold, T., Marwan, N., Drury, A. J., Liebrand, D., Agnini, C., Anagnostou, E., Barnet, J. S. K., Bohaty, S. M., De Vleeschouwer, D., Florindo, F., et al.: An astronomically dated record of Earth's climate and its predictability over the last 66 million years, Science, 369, 1383–1387, 2020.

Wetherald, R. T. and Manabe, S.: The effects of changing the solar constant on the climate of a general circulation model, Journal of the Atmospheric Sciences, 32, 2044–2059, 1975.

Wilkinson, L. and Friendly, M.: The History of the Cluster Heat Map, The American Statistician, 63, 179–184, https://doi.org/10.1198/tas.2009.0033, 2009.

Willeit, M., Ganopolski, A., Calov, R., and Brovkin, V.: Mid-Pleistocene transition in glacial cycles explained by declining CO2 and regolith removal, Science Advances, 5, eaav7337, 2019.

Zhang, G., Liu, Z., and Ma, Z.: Generalized synchronization of different dimensional chaotic dynamical systems, Chaos, Solitons & Fractals, 32, 773–779, https://doi.org/10.1016/j.chaos.2005.11.099, 2007.